doi: 10.82124/CEAS-GNC-2026-076 CEAS-GNC-2026-076

Hybrid Lyapunov and Barrier Function-Based Control for Guaranteed Spacecraft Rendezvous and Docking

Hugo Matias PhD Candidate, Center of Technology and Systems (UNINOVA-CTS), NOVA School of Science and Technology (NOVA-FCT), Department of Electrical and Computer Engineering, 2829-516 Caparica, Portugal. h.matias@campus.fct.unl.pt
Doctoral Researcher, Institute for Systems and Robotics (ISR-Lisbon), Instituto Superior Técnico (IST), 1049-001 Lisbon, Portugal.

Daniel Silvestre Assistant Professor, Center of Technology and Systems (UNINOVA-CTS), NOVA School of Science and Technology (NOVA-FCT), Department of Electrical and Computer Engineering, 2829-516 Caparica, Portugal. dsilvestre@fct.unl.pt
Researcher, Institute for Systems and Robotics (ISR-Lisbon), Instituto Superior Técnico (IST), 1049-001 Lisbon, Portugal.

ABSTRACT

This paper addresses the problem of controlling a chaser spacecraft to safely achieve rendezvous and docking with a target spacecraft, whose geometry is modeled as a bounded nonconvex polytope. Currently, a natural solution approach is to design a Control Lyapunov Function (CLF) and a single Control Barrier Function (CBF), and then apply the standard CLF-CBF Quadratic Program (QP)-based framework to encode the stabilization and safety objectives into a single controller. However, a major limitation of the standard CLF-CBF-QP approach is the emergence of undesired equilibrium points that lead to deadlock situations and preclude task completion. This issue is even more critical in the present setting, owing to the nonconvex nature of the problem. To overcome this drawback, this paper proposes a hybrid CLF-CBF control strategy that ensures safe global navigation to the docking point, improving upon current alternatives in the literature, which are limited to convex obstacle sets. The proposed approach is validated in a high-fidelity spacecraft rendezvous and docking scenario, demonstrating its effectiveness under realistic mission conditions.

Keywords: Spacecraft Rendezvous and Docking, Control Barrier Functions, Hybrid Feedback, Backstepping

1 Introduction

A common requirement in spacecraft operations is the capability of one spacecraft, called the chaser, to achieve rendezvous and docking with another spacecraft, referred to as the target. These maneuvers are fundamental in a broad range of space missions, including Active Debris Removal (ADR) [1], On-Orbit Servicing, Assembly, and Manufacturing (OSAM) operations [2], [3], as well as crew and cargo resupply for space stations [4]. At its core, successful rendezvous and docking requires the chaser spacecraft to converge to a designated docking point while avoiding collision with the target spacecraft.

Autonomous spacecraft rendezvous and docking have been addressed using several techniques, with potential field methods standing out among the classical approaches [5], [6], [7], [8]. A potential field is a scalar function whose gradient drives the system toward the desired equilibrium point and away from the unsafe set. However, while conceptually simple, these methods face several limitations. Most notably,

Except where otherwise noted, content of this paper is licensed under a Creative Commons Attribution 4.0 International License.

The reproduction and distribution with attribution of the entire paper or of individual pages, in electronic or printed form, including any material under non-CC-BY 4.0 licenses is hereby granted by the authors and respective copyright owners.

such methods introduce spurious equilibrium points that prevent global convergence, and they lack the flexibility to accommodate additional mission constraints. Moreover, they are prone to other drawbacks, such as oscillatory motion, overly conservative trajectories, and difficult parameter tuning [9].

Over the last decades, Model Predictive Control (MPC) has gained considerable attention for spacecraft rendezvous and docking [10], [11], [12], [13], [14]. MPC optimizes a cost function over a prediction horizon at each time step while explicitly accounting for state and input constraints. However, the nonlinear nature of spacecraft dynamics and nonconvex sets for the admissible states place MPC within the realm of nonconvex optimization, with all its associated challenges. Consequently, despite its predictive advantages, MPC imposes a substantial computational load for real-time execution, even when resorting to convexification techniques [15]. Moreover, the onboard computational power is usually limited by the available power budget and radiation-hardening requirements, further challenging the use of MPC [16].

In the past decade, Control Barrier Functions (CBFs) have emerged as a promising tool for designing controllers with formal safety guarantees for nonlinear systems [17], [18]. CBFs generalize the concept of Control Lyapunov Functions (CLFs) [19] for safety, where the key point is imposing a Lyapunov-like condition on the time derivative of a CBF to ensure forward invariance of the safe set. For control-affine systems, CLFs and CBFs can be unified by means of Quadratic Programs (QPs), effectively combining stabilization and safety objectives [17]. Under this approach, the conditions for asymptotic stability and safety arise from the time derivatives of the CLF and CBF, which depend linearly on the control input. As a result, controllers can be designed using QPs with linear inequality constraints, which can be efficiently solved in real time. This approach has been effectively applied in the space context, particularly for safe spacecraft reorientation under pointing constraints [20], [21]. However, its application to rendezvous and docking remains limited. A notable example is the work in [22], which introduces a robust CBF method to handle bounded disturbances, but only considers a simple planetary landing scenario.

Moreover, the standard CLF-CBF-QP framework has a significant limitation. While it enforces the forward invariance of the safe set with a hard constraint, it relaxes the stabilization objective to maintain the feasibility of the QP. This leads to the emergence of undesired equilibrium points that cause deadlock situations and preclude any guarantees of task completion [23], [24], closely mirroring the similar issue found in potential field methods.

A few works have addressed deadlock resolution in the context of CBF-based control. For instance, [25] introduces Control Lyapunov Barrier Functions (CLBFs) to ensure safe global asymptotic stabilization. However, as shown in [26], there cannot exist a CLBF that renders a point globally asymptotically stable while avoiding a bounded set. In [23], the authors propose mitigating the unwanted equilibria by combining CBFs with asymmetric rotating CLFs. However, despite rendering the unwanted equilibrium points unstable, the authors do not provide global convergence guarantees, and this approach may induce undesired oscillations. Later, [27] shows that the interior spurious equilibria can be eliminated using a nominal stabilizing controller, but does not address the more challenging boundary equilibria.

Recently, deadlock resolution in the CBF-based setting has been addressed via hybrid feedback, as continuous control approaches present a greater difficulty in handling this issue [28]. Particularly, hybrid CBF formulations, originally developed for hybrid systems [29], [30], have been proposed for deadlock resolution in continuous-time systems, where decisiveness is achieved by combining CBFs with logic variables. For example, in [31], [32], and [33], the authors propose the use of an avoidance shell defined by two partially overlapping domains, where decisiveness is achieved by switching between the domains. However, the avoidance shell is an overly conservative obstacle representation.

More recently, in [34], the authors propose a hybrid CBF approach based on a polytopic avoidance domain, offering a less conservative obstacle representation, where deadlock resolution is achieved through a switching mechanism similar to that from synergistic Lyapunov functions [35], [36]. Nevertheless, the approach from [34] also lacks flexibility, as deadlock resolution is restricted to specific convex polytopes, which themselves depend on the desired equilibrium point.

Except where otherwise noted, content of this paper is licensed under a Creative Commons Attribution 4.0 International License.

The reproduction and distribution with attribution of the entire paper or of individual pages, in electronic or printed form, including any material under non-CC-BY 4.0 licenses is hereby granted by the authors and respective copyright owners.

To overcome the limitations of the previous methods, our recent work in [37] introduces an improved hybrid CLF-CBF framework that guarantees safe global navigation in environments with arbitrary convex polytopic obstacles, providing a systematic and flexible design. The approach decomposes the navigation task into a sequence of safe stabilization subproblems (the hybrid modes), each defined by an active safe half-space and an associated target point, and for each subproblem, a controller designed using compatible CLF and CBF constraints ensures convergence to the active setpoint. As the trajectory approaches the active setpoint, a switching mechanism updates the active safe half-space and assigns a new target point. Global navigation is then achieved by ensuring that the switching logic generates a sequence of setpoints converging to the desired goal point. The method is developed for first-order systems and extended to higher-order dynamics via a joint CLF-CBF backstepping procedure. Nonetheless, this approach remains limited to convex polytopic obstacles.

1.1 Main Contributions and Organization

This paper considers the problem of controlling a chaser spacecraft to safely achieve rendezvous and docking with an orbiting target spacecraft. The geometry of the target spacecraft is modeled as a bounded nonconvex polytope, defined as a bounded convex polytope with a convex docking port. To address this problem, we propose a hybrid CLF-CBF control strategy that guarantees safe global navigation to the desired docking point, extending our work in [37] to environments with nonconvex polytopic obstacles.

The main contributions of this paper can be summarized as follows:

- We extend the hybrid CLF-CBF framework from [37] to environments with nonconvex polytopic obstacles and also time-varying system dynamics;
- We validate the proposed approach in a high-fidelity spacecraft rendezvous and docking scenario, demonstrating its effectiveness under realistic mission conditions.

The remainder of this paper is structured as follows. Section 2 provides important background on CLFs and CBFs, and Section 3 formulates the rendezvous and docking problem addressed in this paper. Section 4 presents the proposed hybrid CLF-CBF control strategy, with simulation results in Section 5. Finally, Section 6 summarizes conclusions and future directions.

1.2 Notation and General Definitions

$\mathbb{N}$ is the set of nonnegative integers. $\mathbb{R}$, $\mathbb{R}_{\geq 0}$, and $\mathbb{R}_{>0}$ are the sets of real, nonnegative, and positive numbers, respectively. $\mathbb{R}^n$ is the n-dimensional euclidean space, and $\mathbb{S}^{n-1}$ is the unit sphere in $\mathbb{R}^n$. $\mathbb{R}^{n\times m}$ is the set of $n \times m$ real matrices, $\mathbb{R}^{n\times n}_{\succ 0}$ is the set of positive-definite matrices of size n, and $\mathrm{SO}(n)$ is the special orthogonal group in $\mathbb{R}^n$. For a given set $\mathcal{S} \subseteq \mathbb{R}^n$, $\mathrm{int}(\mathcal{S})$ and $\partial\mathcal{S}$ are the interior and boundary of $\mathcal{S}$, respectively. The p-norm of a vector $\mathbf{x} \in \mathbb{R}^n$ is denoted as $\|\mathbf{x}\|_p$, with $\|\mathbf{x}\| = \|\mathbf{x}\|_2$, and for two vectors $\mathbf{x}_1 \in \mathbb{R}^{n_1}$, $\mathbf{x}_2 \in \mathbb{R}^{n_2}$, we often use the notation $(\mathbf{x}_1, \mathbf{x}_2) = \left[\mathbf{x}_1^\top \; \mathbf{x}_2^\top\right]^\top \in \mathbb{R}^{n_1+n_2}$. For a differentiable function $h : \mathbb{R}^n \to \mathbb{R}$ and $\mathbf{G} : \mathbb{R}^n \times \mathbb{R}_{\geq 0} \to \mathbb{R}^{n\times m}$, we use the Lie-derivative notation $(L_{\mathbf{G}}h)(\mathbf{x}, t) = \nabla h(\mathbf{x})^\top \mathbf{G}(\mathbf{x}, t)$. Additionally, $\dot{\mathbf{x}}$ is the time derivative of $\mathbf{x}$, and $\mathbf{x}^+$ is the value of $\mathbf{x}$ after an instantaneous change. Finally, $\mathbf{0}_{n\times m}$ is the $n \times m$ matrix of zeros, and $\mathbf{I}_n$ is the identity matrix of size n (dimensions are often omitted).

Definition 1 (Class-$\mathcal{K}$/$\mathcal{K}_\infty$ Function) *A continuous function $\gamma : \mathbb{R}_{\geq 0} \to \mathbb{R}_{\geq 0}$ is a class-$\mathcal{K}$ function if it is strictly increasing with $\gamma(0) = 0$, and it is a class-$\mathcal{K}_\infty$ function if, additionally, $\lim_{s\to\infty} \gamma(s) = \infty$.*

Definition 2 (Extended Class-$\mathcal{K}$/$\mathcal{K}_\infty$ Function) *A continuous function $\alpha : \mathbb{R} \to \mathbb{R}$ is an extended class-$\mathcal{K}$ function if it is strictly increasing with $\alpha(0) = 0$, and it is an extended class-$\mathcal{K}_\infty$ function if, additionally, we have $\lim_{s\to\pm\infty} \alpha(s) = \pm\infty$.*

Definition 3 (Positive-Definite Function around a Point) *A scalar function $V : \mathbb{R}^n \to \mathbb{R}_{\geq 0}$ is said to be positive definite around a point $\bar{\mathbf{x}}$ if $V(\bar{\mathbf{x}}) = 0$ and $V(\mathbf{x}) > 0$ for all $\mathbf{x} \in \mathbb{R}^n \setminus \{\bar{\mathbf{x}}\}$.*

Except where otherwise noted, content of this paper is licensed under a Creative Commons Attribution 4.0 International License.

The reproduction and distribution with attribution of the entire paper or of individual pages, in electronic or printed form, including any material under non-CC-BY 4.0 licenses is hereby granted by the authors and respective copyright owners.

2 Mathematical Background

Consider a time-varying control-affine system of the form

$$\dot{\mathbf{x}} = \mathbf{f}(\mathbf{x}, t) + \mathbf{G}(\mathbf{x}, t)\mathbf{u}, \tag{1}$$

where $\mathbf{x} \in \mathbb{R}^n$ is the system state, $\mathbf{u} \in \mathbb{R}^m$ is the control input, and the functions $\mathbf{f} : \mathbb{R}^n \times \mathbb{R}_{\geq 0} \to \mathbb{R}^n$ and $\mathbf{G} : \mathbb{R}^n \times \mathbb{R}_{\geq 0} \to \mathbb{R}^{n \times m}$ are locally Lipschitz in $\mathbf{x}$ and continuous in t. Applying a feedback controller $\mathbf{k} : \mathbb{R}^n \times \mathbb{R}_{\geq 0} \to \mathbb{R}^m$ to (1) yields the time-varying closed-loop system

$$\dot{\mathbf{x}} = \mathbf{f}(\mathbf{x}, t) + \mathbf{G}(\mathbf{x}, t)\mathbf{k}(\mathbf{x}, t). \tag{2}$$

As the functions $\mathbf{f}$ and $\mathbf{G}$ are locally Lipschitz in $\mathbf{x}$ and continuous in t, if the controller $\mathbf{k}$ also satisfies these properties, then, for every initial condition $\mathbf{x}_0 \in \mathbb{R}^n$, there exists a unique continuously differentiable solution $\boldsymbol{\varphi} : I(\mathbf{x}_0) \to \mathbb{R}^n$ satisfying

$$\begin{aligned} \dot{\boldsymbol{\varphi}}(t) &= \mathbf{f}(\boldsymbol{\varphi}(t), t) + \mathbf{G}(\boldsymbol{\varphi}(t), t)\mathbf{k}(\boldsymbol{\varphi}(t), t), \\ \boldsymbol{\varphi}(0) &= \mathbf{x}_0, \end{aligned} \tag{3}$$

for all $t \in I(\mathbf{x}_0)$, where $I(\mathbf{x}_0) \subseteq \mathbb{R}_{\geq 0}$ denotes the maximal interval of existence for the solution [38]. If $I(\mathbf{x}_0) = \mathbb{R}_{\geq 0}$, the solution is said to be complete. Next, we define the notions of asymptotic stability and forward invariance considered in this paper.

Definition 4 (Asymptotic Stability) *An equilibrium point $\bar{\mathbf{x}}$ of the system* (2) *is asymptotically stable if it is stable and there exists a maximal set $\mathcal{A} \supset \{\bar{\mathbf{x}}\}$ such that, for every initial condition $\mathbf{x}_0 \in \mathcal{A}$, $\boldsymbol{\varphi}$ is complete and $\lim_{t \to \infty} \|\boldsymbol{\varphi}(t) - \bar{\mathbf{x}}\| = 0$. The set $\mathcal{A}$ is called the region of attraction of $\bar{\mathbf{x}}$. If $\mathcal{A} = \mathbb{R}^n$, then $\bar{\mathbf{x}}$ is said to be globally asymptotically stable.*

Definition 5 (Forward Invariance) *A set $C \subset \mathbb{R}^n$ is said to be forward invariant for the system* (2) *if, for every initial condition $\mathbf{x}_0 \in C$, we have $\boldsymbol{\varphi}(t) \in C$ for all $t \in I(\mathbf{x}_0)$.*

2.1 Control Lyapunov and Control Barrier Functions

We begin by considering the usual control objective of globally asymptotically stabilizing the system (1) to a desired equilibrium point $\bar{\mathbf{x}}$. This can be achieved by designing a control law that drives a proper and positive-definite function (around $\bar{\mathbf{x}}$) $V : \mathbb{R}^n \to \mathbb{R}_{\geq 0}$ to zero, motivating the concept of CLF [39].

Definition 6 (CLF) *A continuously differentiable, proper, and positive-definite function $V : \mathbb{R}^n \to \mathbb{R}_{\geq 0}$ around a point $\bar{\mathbf{x}}$ is a CLF for the system* (1) *if there exists a class-$\mathcal{K}$ function $\gamma : \mathbb{R}_{\geq 0} \to \mathbb{R}_{\geq 0}$ such that, for all $(\mathbf{x}, t) \in (\mathbb{R}^n \setminus \{\bar{\mathbf{x}}\}) \times \mathbb{R}_{\geq 0}$,*

$$\inf_{\mathbf{u} \in \mathbb{R}^m} \left[(L_{\mathbf{f}} V)(\mathbf{x}, t) + (L_{\mathbf{G}} V)(\mathbf{x}, t)\mathbf{u} \right] < -\gamma(V(\mathbf{x})). \tag{4}$$

Given a CLF V for (1) and an associated class-$\mathcal{K}$ function γ, we define the pointwise set of controls

$$K_{\mathrm{CLF}}(\mathbf{x}, t) = \{\mathbf{u} \in \mathbb{R}^m : (L_{\mathbf{f}} V)(\mathbf{x}, t) + (L_{\mathbf{G}} V)(\mathbf{x}, t)\mathbf{u} \leq -\gamma(V(\mathbf{x}))\}. \tag{5}$$

This yields the following main result with respect to CLFs.

Theorem 1 (Stabilizing Controller [39]) *Let $V : \mathbb{R}^n \to \mathbb{R}_{\geq 0}$ be a continuously differentiable, proper, and positive-definite function around a point $\bar{\mathbf{x}}$. If V is a CLF for* (1)*, then the set $K_{\mathrm{CLF}}(\mathbf{x}, t)$ is nonempty for all $(\mathbf{x}, t) \in \mathbb{R}^n \times \mathbb{R}_{\geq 0}$, and any controller $\mathbf{k} : \mathbb{R}^n \times \mathbb{R}_{\geq 0} \to \mathbb{R}^m$ that is locally Lipschitz in $\mathbf{x}$, continuous in t, and with $\mathbf{k}(\mathbf{x}, t) \in K_{\mathrm{CLF}}(\mathbf{x}, t)$ for all $(\mathbf{x}, t) \in \mathbb{R}^n \times \mathbb{R}_{\geq 0}$ globally asymptotically stabilizes* (1) *to $\bar{\mathbf{x}}$.*

Except where otherwise noted, content of this paper is licensed under a Creative Commons Attribution 4.0 International License.

The reproduction and distribution with attribution of the entire paper or of individual pages, in electronic or printed form, including any material under non-CC-BY 4.0 licenses is hereby granted by the authors and respective copyright owners.

Additionally, we now consider the safety objective of rendering a given safe set forward invariant. Particularly, we consider a safe set $C \subset \mathbb{R}^n$ defined as the 0-superlevel set of a continuously differentiable function $h : \mathbb{R}^n \to \mathbb{R}$ with $\nabla h(\mathbf{x}) \neq \mathbf{0}$ when $h(\mathbf{x}) = 0$, yielding

$$\begin{aligned} C &= \{\mathbf{x} \in \mathbb{R}^n : h(\mathbf{x}) \geq 0\}, \\ \partial C &= \{\mathbf{x} \in \mathbb{R}^n : h(\mathbf{x}) = 0\}, \\ \text{int}(C) &= \{\mathbf{x} \in \mathbb{R}^n : h(\mathbf{x}) > 0\}. \end{aligned} \tag{6}$$

If h has the properties of a CBF, then it can be used to design safe controllers for the system (1).

Definition 7 (CBF [17]) *Let $C \subset \mathbb{R}^n$ be the 0-superlevel set of a continuously differentiable function $h : \mathbb{R}^n \to \mathbb{R}$ with $\nabla h(\mathbf{x}) \neq \mathbf{0}$ when $h(\mathbf{x}) = 0$. The function h is a (zeroing) CBF for the system* (1) *if there exists an extended class-$\mathcal{K}_\infty$ function $\alpha : \mathbb{R} \to \mathbb{R}$ such that, for all $(\mathbf{x}, t) \in \mathbb{R}^n \times \mathbb{R}_{\geq 0}$,*

$$\sup_{\mathbf{u} \in \mathbb{R}^m} [(L_{\mathbf{f}} h)(\mathbf{x}, t) + (L_{\mathbf{G}} h)(\mathbf{x}, t)\mathbf{u}] > -\alpha(h(\mathbf{x})). \tag{7}$$

This definition means that a CBF is allowed to decrease in the interior of the safe set but not on its boundary. Similar to CLFs, given a CBF h for (1) and a corresponding extended class-$\mathcal{K}_\infty$ function α, we define the pointwise set of controls

$$K_{\text{CBF}}(\mathbf{x}, t) = \{\mathbf{u} \in \mathbb{R}^m : (L_{\mathbf{f}} h)(\mathbf{x}, t) + (L_{\mathbf{G}} h)(\mathbf{x}, t)\mathbf{u} \geq -\alpha(h(\mathbf{x}))\}. \tag{8}$$

This yields the following main result concerning CBFs.

Theorem 2 (Safe Controller [17]) *Let $C \subset \mathbb{R}^n$ be the 0-superlevel set of a continuously differentiable function $h : \mathbb{R}^n \to \mathbb{R}$ with $\nabla h(\mathbf{x}) \neq \mathbf{0}$ when $h(\mathbf{x}) = 0$. If the function h is a CBF for the system* (1)*, then the set $K_{\text{CBF}}(\mathbf{x}, t)$ is nonempty for all $(\mathbf{x}, t) \in \mathbb{R}^n \times \mathbb{R}_{\geq 0}$, and any controller $\mathbf{k} : \mathbb{R}^n \times \mathbb{R}_{\geq 0} \to \mathbb{R}^m$ that is locally Lipschitz in $\mathbf{x}$, continuous in t, and with $\mathbf{k}(\mathbf{x}, t) \in K_{\text{CBF}}(\mathbf{x}, t)$ for all $(\mathbf{x}, t) \in \mathbb{R}^n \times \mathbb{R}_{\geq 0}$ renders C forward invariant for the resulting closed-loop system. Also, C becomes asymptotically stable in $\mathbb{R}^n$.*

Remark 1 *The strictness of the inequalities in* (4) *and* (7) *enables proving that optimization-based controllers relying on CLFs and CBFs are locally Lipschitz in $\mathbf{x}$ [40], [41].*

2.2 Quadratic Program Formulation

Stabilization and safety objectives represented by CLFs and CBFs can be unified via an optimization-based approach. Specifically, given a CLF V and a CBF h associated with a safe set, the standard approach for encoding these objectives into a controller $\mathbf{k} : \mathbb{R}^n \times \mathbb{R}_{\geq 0} \to \mathbb{R}^m$ is through the following QP:

$$\begin{aligned} (\mathbf{k}(\mathbf{x}, t), \cdot) = \underset{(\mathbf{u}, \delta) \in \mathbb{R}^{m+1}}{\arg\min}\ & \frac{1}{2}\|\mathbf{u} - \mathbf{k}_{\text{n}}(\mathbf{x}, t)\|^2 + \frac{1}{2} p \delta^2 \\ \text{subject to}\ & (L_{\mathbf{f}} V)(\mathbf{x}, t) + (L_{\mathbf{G}} V)(\mathbf{x}, t)\mathbf{u} \leq -\gamma(V(\mathbf{x})) + \delta, \\ & (L_{\mathbf{f}} h)(\mathbf{x}, t) + (L_{\mathbf{G}} h)(\mathbf{x}, t)\mathbf{u} \geq -\alpha(h(\mathbf{x})), \end{aligned} \tag{9}$$

where $\mathbf{k}_{\text{n}} : \mathbb{R}^n \times \mathbb{R}_{\geq 0} \to \mathbb{R}^m$ denotes a nominal controller that does not necessarily ensure stability and safety, $p \in \mathbb{R}_{>0}$ is a scaling parameter, γ is a class-$\mathcal{K}$ function corresponding to the CLF, and α is an extended class-$\mathcal{K}_\infty$ function associated with the CBF. The CBF constraint ensures the forward invariance of the safe set, and the relaxation variable δ softens the stabilization objective to maintain the feasibility of the optimization problem across all $\mathbf{x} \in \mathbb{R}^n$. Also, the controller defined in (9) can be expressed in closed form via the Karush-Kuhn-Tucker (KKT) conditions, and it is locally Lipschitz in $\mathbf{x}$ and continuous in t if $\mathbf{k}_{\text{n}}$ has such properties and the CLF and CBF gradients, along with γ and α, are locally Lipschitz [37].

Except where otherwise noted, content of this paper is licensed under a Creative Commons Attribution 4.0 International License.

The reproduction and distribution with attribution of the entire paper or of individual pages, in electronic or printed form, including any material under non-CC-BY 4.0 licenses is hereby granted by the authors and respective copyright owners.

When input bounds must also be taken into account, an improved formulation is required, as simply augmenting the QP from (9) with the input constraints may render the resulting QP infeasible. To properly account for input bounds described by a compact convex set $\mathcal{U} \subset \mathbb{R}^m$, a suitable approach is to adopt the optimal-decay formulation from [42] and design a controller $\mathbf{k}$ through the following QP:

$$\begin{aligned}(\mathbf{k}(\mathbf{x},t),\cdot,\cdot) = \underset{(\mathbf{u},\delta,\omega)\in\mathbb{R}^{m+2}}{\arg\min}\ & \frac{1}{2}\|\mathbf{u}-\mathbf{k}_{\mathrm{n}}(\mathbf{x},t)\|^2 + \frac{1}{2}p\delta^2 + \frac{1}{2}p_\omega(\omega-1)^2 \\ \text{subject to}\ & (L_{\mathbf{f}}V)(\mathbf{x},t) + (L_{\mathbf{G}}V)(\mathbf{x},t)\mathbf{u} \le -\gamma(V(\mathbf{x})) + \delta, \\ & (L_{\mathbf{f}}h)(\mathbf{x},t) + (L_{\mathbf{G}}h)(\mathbf{x},t)\mathbf{u} \ge -\omega\alpha(h(\mathbf{x})), \\ & \mathbf{u}\in\mathcal{U},\end{aligned} \tag{10}$$

with scaling parameters $p, p_\omega \in \mathbb{R}_{>0}$. This formulation guarantees feasibility when $h(\mathbf{x}) \neq 0$.

However, it is important to highlight that a significant limitation of the standard CLF-CBF approaches (and continuous navigation methods in general) is the emergence of additional equilibrium points beyond the zero of the CLF. These undesired equilibrium points can trap the system and prevent global convergence to the desired equilibrium point. To overcome this issue, our recent work in [37] proposes a hybrid CLF-CBF control framework that guarantees safe global navigation in environments with bounded obstacles represented as convex polytopes, improving upon the hybrid approaches from [33] and [34].

3 Problem Formulation

We consider the problem of controlling a chaser spacecraft to safely perform rendezvous and docking with an orbiting target spacecraft. The target spacecraft is fitted with a body-fixed reference frame $\mathcal{F}_{\mathrm{T}}$, in which the chaser dynamics are described by a second-order strict-feedback model of the form

$$\dot{\mathbf{p}} = \mathbf{v}, \tag{11}$$

$$\dot{\mathbf{v}} = \mathbf{f}_1(\mathbf{p},\mathbf{v},t) + \mathbf{G}_1(\mathbf{p},\mathbf{v},t)\mathbf{u}, \tag{12}$$

where $\mathbf{p}, \mathbf{v} \in \mathbb{R}^p$ denote the position and velocity of the chaser in $\mathcal{F}_{\mathrm{T}}$, respectively, $\mathbf{u} \in \mathbb{R}^m$ is the control input, the functions $\mathbf{f}_1 : \mathbb{R}^p \times \mathbb{R}^p \times \mathbb{R}_{\ge 0} \to \mathbb{R}^p$ and $\mathbf{G}_1 : \mathbb{R}^p \times \mathbb{R}^p \times \mathbb{R}_{\ge 0} \to \mathbb{R}^{p\times m}$ are locally Lipschitz in $(\mathbf{p},\mathbf{v})$ and continuous in t, and $\mathbf{G}_1(\mathbf{p},\mathbf{v},t)$ has full row rank for all $(\mathbf{p},\mathbf{v},t) \in \mathbb{R}^p \times \mathbb{R}^p \times \mathbb{R}_{\ge 0}$.

The body of the target spacecraft is modeled as a bounded nonconvex polytope $\mathcal{T} \subset \mathbb{R}^p$, defined as

$$\mathcal{T} = \mathcal{P} \setminus \mathcal{D}, \tag{13}$$

where $\mathcal{P} \subset \mathbb{R}^p$ is a bounded convex polytope, and $\mathcal{D} \subset \mathbb{R}^p$ is an unbounded convex polytope that models the docking port, both with nonempty interior. The set $\mathcal{P}$ is defined by the intersection of $Q \ge p+1$ half-space domains as

$$\mathcal{P} = \left\{\mathbf{p} \in \mathbb{R}^p : h_1(\mathbf{p}) < 0 \wedge \cdots \wedge h_Q(\mathbf{p}) < 0\right\}, \tag{14}$$

where, for each $q \in \{1,\ldots,Q\}$, the function $h_q : \mathbb{R}^p \to \mathbb{R}$ is defined for all $\mathbf{p} \in \mathbb{R}^p$ as

$$h_q(\mathbf{p}) = \mathbf{n}_q^\top \mathbf{p} - d_q, \tag{15}$$

with $\mathbf{n}_q \in \mathbb{S}^{p-1}$ denoting the outward-pointing unit normal of facet q and $d_q \in \mathbb{R}$ the respective offset. We further assume that the half-space constraints defining the polytope are nonredundant, so that removing any of them results in a different set. This implies that the normal vectors satisfy $\mathbf{n}_{q_1} \neq \mathbf{n}_{q_2}$ for all distinct $q_1, q_2 \in \{1,\ldots,Q\}$. Similarly, the set $\mathcal{D}$ is defined by the intersection of $M \ge p$ half-spaces as

$$\mathcal{D} = \{\mathbf{p} \in \mathbb{R}^p : \psi_1(\mathbf{p}) \ge 0 \wedge \cdots \wedge \psi_M(\mathbf{p}) \ge 0\}, \tag{16}$$

Except where otherwise noted, content of this paper is licensed under a Creative Commons Attribution 4.0 International License.

The reproduction and distribution with attribution of the entire paper or of individual pages, in electronic or printed form, including any material under non-CC-BY 4.0 licenses is hereby granted by the authors and respective copyright owners.

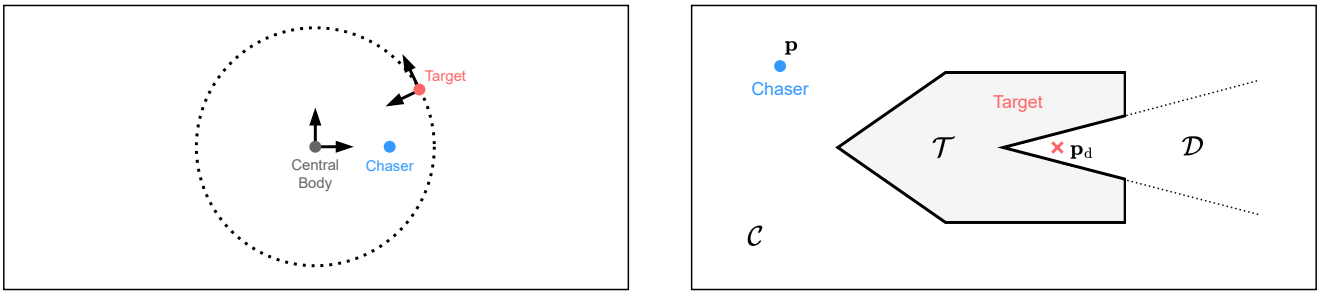

(a) Inertial Frame **(b) Target-Fixed Frame**

Fig. 1 Illustrative problem setup. The left figure depicts a possible setup in an inertial frame centered on a central body around which the target orbits, along with the position of the chaser spacecraft in that frame. The right figure depicts the same setup in the target-fixed frame, with a close-up view that highlights a possible representation of the geometry of the target.

where, for each $i \in \{1, \dots, M\}$, the function $\psi_i : \mathbb{R}^p \to \mathbb{R}$ is defined for all $\mathbf{p} \in \mathbb{R}^p$ as

$$\psi_i(\mathbf{p}) = \mathbf{a}_i^\top \mathbf{p} - b_i, \tag{17}$$

with $\mathbf{a}_i \in \mathbb{S}^{p-1}$ denoting the inward-pointing unit normal of the ith facet and $b_i \in \mathbb{R}$ the associated offset. Given this formulation, the safe set for the position of the chaser spacecraft is defined as

$$\mathcal{C} = \mathbb{R} \setminus \mathcal{T} = \mathbb{R} \setminus (\mathcal{P} \setminus \mathcal{D}) = (\mathbb{R} \setminus \mathcal{P}) \cup \mathcal{D}, \tag{18}$$

where the complement of $\mathcal{P}$ is given by

$$\mathbb{R} \setminus \mathcal{P} = \left\{ \mathbf{p} \in \mathbb{R}^p : h_1(\mathbf{p}) \geq 0 \vee \cdots \vee h_Q(\mathbf{p}) \geq 0 \right\}. \tag{19}$$

An illustrative example of the problem setup under consideration is depicted in Fig. 1. Having the previous setup in place, we are now ready to formally state the problem addressed in this paper.

Problem 1 *Consider the above setup, and let $\mathbf{p}_\mathrm{d} \in \mathcal{P} \cap \mathrm{int}(\mathcal{D})$ be the desired docking point for the chaser spacecraft. Then, assuming an unbounded control input, design a control strategy which, for every initial condition $(\mathbf{p}_0, \mathbf{v}_0) \in \mathrm{int}(\mathcal{C}) \times \mathbb{R}^p$, guarantees that the resulting chaser trajectory $\boldsymbol{\varphi} : \mathbb{R}_{\geq 0} \to \mathbb{R}^p$ satisfies $\lim_{t \to \infty} \|\boldsymbol{\varphi}(t) - \mathbf{p}_\mathrm{d}\| = 0$ and $\boldsymbol{\varphi}(t) \in \mathcal{C}$ for all $t \in \mathbb{R}_{\geq 0}$. Additionally, extend the proposed approach to handle bounded control inputs.*

A straightforward approach to this problem is to construct a single CBF using smooth approximations of the maximum and minimum functions [43], and then apply the standard QP formulations described in Section 2. However, as discussed in Section 2 and shown in [37], this approach gives rise to asymptotically stable undesired equilibria at the boundary of the safe set, leading to deadlock situations and precluding any guarantees of task completion. This limitation is even more critical in the present setup, owing to the nonconvexity of $\mathcal{T}$ and the fact that the docking point is located within the convex hull of $\mathcal{T}$.

4 Hybrid Control Solution

To address the problem outlined in Section 3, we propose a hybrid CLF-CBF control algorithm that builds upon our work from [37], extending it to nonconvex polytopic obstacles and time-varying systems. For greater clarity, we structure the approach into two sequential phases: rendezvous and docking. During the rendezvous phase, we employ the hybrid framework from [37] to safely guide the chaser spacecraft to a point $\bar{\mathbf{p}}$ located on the boundary of $\mathcal{P}$ and within the interior of the docking port, i.e., $\bar{\mathbf{p}} \in \partial\mathcal{P} \cap \mathrm{int}(\mathcal{D})$.

Except where otherwise noted, content of this paper is licensed under a Creative Commons Attribution 4.0 International License.

The reproduction and distribution with attribution of the entire paper or of individual pages, in electronic or printed form, including any material under non-CC-BY 4.0 licenses is hereby granted by the authors and respective copyright owners.

Once the spacecraft reaches a specified neighborhood of $\bar{\mathbf{p}}$, the algorithm switches to the docking mode, with the control law safely stabilizing the chaser spacecraft to the desired docking point $\mathbf{p}_\mathrm{d}$.

In the rendezvous phase, the safe set for the position of the chaser is defined as $\mathbb{R} \setminus \mathcal{P}$, and the control strategy involves solving a sequence of safe stabilization subproblems. Each subproblem consists of an active safe half-space and an associated target point, for which we design a controller using compatible CLF and CBF constraints, ensuring convergence to the active setpoint. As the spacecraft approaches the current target, a switching mechanism updates the active half-space and assigns a new setpoint. Global convergence to $\bar{\mathbf{p}}$ is then achieved by ensuring that the resulting sequence of setpoints converges to $\bar{\mathbf{p}}$.

During the rendezvous phase, the control strategy can then be described through an auxiliary hybrid system with flow dynamics of the form

$$\begin{bmatrix} \dot{\mathbf{p}} \\ \dot{\mathbf{v}} \\ \dot{\boldsymbol{\xi}} \end{bmatrix} = \begin{bmatrix} \mathbf{v} \\ \mathbf{f}_1(\mathbf{p}, \mathbf{v}, t) + \mathbf{G}_1(\mathbf{p}, \mathbf{v}, t)\mathbf{k}_{\boldsymbol{\xi},1}(\mathbf{p}, \mathbf{v}, t) \\ \mathbf{0} \end{bmatrix}, \quad (\mathbf{p}, \boldsymbol{\xi}) \in \mathcal{F}, \tag{20}$$

and with jump dynamics described by

$$\begin{bmatrix} \mathbf{p}^+ \\ \mathbf{v}^+ \\ \boldsymbol{\xi}^+ \end{bmatrix} = \begin{bmatrix} \mathbf{p} \\ \mathbf{v} \\ \mathbf{s}(\mathbf{p}, \boldsymbol{\xi}) \end{bmatrix}, \quad (\mathbf{p}, \boldsymbol{\xi}) \in \mathcal{J}. \tag{21}$$

In the above, $\boldsymbol{\xi} = (\hat{\mathbf{p}}, q) \in \Xi$ is an auxiliary state that includes the active target point, $\hat{\mathbf{p}}$, and the index q of the active safe half-space, with the set $\Xi \subset \mathbb{R}^p \times \{1, \ldots, Q\}$ being defined as

$$\Xi = \left\{ (\hat{\mathbf{p}}, q) \in \mathbb{R}^p \times \{1, \ldots, Q\} : h_q(\hat{\mathbf{p}}) \geq 0 \right\}. \tag{22}$$

Furthermore, $\mathbf{k}_{\boldsymbol{\xi},1} : \mathbb{R}^p \times \mathbb{R}^p \times \mathbb{R}_{\geq 0} \to \mathbb{R}^m$ denotes a controller that solves the subproblem defined by the auxiliary state $\boldsymbol{\xi}$. More specifically, $\mathbf{k}_{\boldsymbol{\xi},1}$ ensures that the chaser remains within the active safe half-space q while guiding it toward the current setpoint $\hat{\mathbf{p}}$. As detailed later, $\mathbf{k}_{\boldsymbol{\xi},1}$ is designed using compatible CLF and CBF constraints, which becomes feasible due to the linear nature of a half-space. The switching logic is defined by the flow and jump sets, $\mathcal{F}, \mathcal{J} \subset \mathbb{R}^p \times \Xi$, together with the update function $\mathbf{s} : \mathcal{J} \to \Xi$. The design of the subproblem controller and the proposed switching logic are detailed in the next subsections.

Once the chaser spacecraft enters a neighborhood of the rendezvous point $\bar{\mathbf{p}}$, i.e., when $\|\mathbf{p} - \bar{\mathbf{p}}\| \leq r$ (with $r \in \mathbb{R}_{>0}$ and this neighborhood included by $\mathrm{int}(\mathcal{D})$), the algorithm switches to the docking mode. In this phase, the active controller becomes $\mathbf{k}_{\mathrm{d},1} : \mathbb{R}^p \times \mathbb{R}^p \times \mathbb{R}_{\geq 0} \to \mathbb{R}^m$, which is a controller that keeps the spacecraft inside $\mathcal{D}$ while guiding it to the docking point $\mathbf{p}_\mathrm{d}$. This controller is also designed using compatible CLF and CBF constraints, which is possible due to the convex and unbounded nature of $\mathcal{D}$.

4.1 Switching Logic

In line with [37], the switching logic of the rendezvous phase relies on a reference direction that serves to guide the sequence of setpoints toward $\bar{\mathbf{p}}$ (see Fig. 2). This direction is defined by the vector

$$\mathbf{w} = \mathbf{n}_{\bar{q}}, \tag{23}$$

where $\bar{q}$ denotes the index of the function h_q attaining the highest value at $\bar{\mathbf{p}}$, meaning that[1]

$$\bar{q} = \underset{q' \in \{1,\ldots,Q\}}{\arg\max}\, h_{q'}(\bar{\mathbf{p}}). \tag{24}$$

[1] We consider that arg max/min returns a single solution when the optimization problem has multiple solutions.

Except where otherwise noted, content of this paper is licensed under a Creative Commons Attribution 4.0 International License.

The reproduction and distribution with attribution of the entire paper or of individual pages, in electronic or printed form, including any material under non-CC-BY 4.0 licenses is hereby granted by the authors and respective copyright owners.

Additionally, for a hybrid mode defined by an active safe half-space q and an active setpoint $\hat{\mathbf{p}}$, we define an auxiliary safe half-space $\hat{q}$, which "forecasts" the safe half-space that will be activated at an upcoming jump event. This auxiliary half-space is defined through

$$\hat{q} = \underset{q' \in \hat{\mathcal{Q}}_q}{\arg\max}\, h_{q'}(\hat{\mathbf{p}}), \tag{25}$$

where $\hat{\mathcal{Q}}_q$ is a subset of half-space indices defined as

$$\hat{\mathcal{Q}}_q = \left\{ q' \in \{1, \ldots, Q\} : \mathbf{w}^\top \mathbf{n}_{q'} > \mathbf{w}^\top \mathbf{n}_q \right\} \cup \{\bar{q}\}. \tag{26}$$

This construction guarantees that the safe half-space $\hat{q}$ is chosen from the safe half-spaces whose normal vectors are more aligned with the reference normal $\mathbf{w} = \mathbf{n}_{\bar{q}}$ than the active one, and the union with $\{\bar{q}\}$ ensures that the set $\hat{\mathcal{Q}}_q$ remains nonempty when the active safe half-space is already $\bar{q}$.

Building on the previous auxiliary variables, the switching logic follows a hysteretic behavior inspired by synergistic Lyapunov functions [35], [36]. More specifically, for an active safe half-space q that does not contain $\bar{\mathbf{p}}$, we will enforce the active setpoint to be placed on the active boundary hyperplane, i.e.,

$$h_q(\hat{\mathbf{p}}) = 0. \tag{27}$$

Moreover, we consider a minimum synergy gap $\mu \in \mathbb{R}_{>0}$, used as a reference for placing the intermediate setpoint relative to the safe half-space $\hat{q}$. Specifically, in addition to (27), we will also enforce that

$$h_{\hat{q}}(\hat{\mathbf{p}}) \geq \mu. \tag{28}$$

This ensures that the intermediate setpoint lies within the interior of the safe half-space $\hat{q}$, with μ defining the minimum allowed distance to the boundary hyperplane $\hat{q}$.

Given this setup and a desired hysteresis width $\sigma \in (0, \mu)$, we define the flow and jump sets as

$$\begin{aligned} \mathcal{F} &= \left\{ (\mathbf{p}, \boldsymbol{\xi}) \in \mathbb{R}^p \times \Xi : h_{\hat{q}}(\mathbf{p}) - h_q(\mathbf{p}) < \sigma \vee h_q(\mathbf{p}) < 0 \right\}, \\ \mathcal{J} &= \left\{ (\mathbf{p}, \boldsymbol{\xi}) \in \mathbb{R}^p \times \Xi : h_{\hat{q}}(\mathbf{p}) - h_q(\mathbf{p}) \geq \sigma \wedge h_q(\mathbf{p}) \geq 0 \right\}, \end{aligned} \tag{29}$$

and the active safe half-space is updated according to

$$q^+ = \hat{q}, \quad \text{if } (\mathbf{p}, \boldsymbol{\xi}) \in \mathcal{J}. \tag{30}$$

This formulation guarantees that safety is maintained when a jump occurs, as from the jump set definition we have $h_{q^+}(\mathbf{p}) \geq h_q(\mathbf{p}) + \sigma > 0$. It also ensures that $\mathbf{w}^\top \mathbf{n}_{q^+} > \mathbf{w}^\top \mathbf{n}_q$, meaning that the alignment of the active normal with the reference one increases with each jump. It now remains to explain how the intermediate target points are computed to enforce the conditions in (27) and (28).

To compute the intermediate setpoints, we assign a tangent direction to each boundary hyperplane other than the reference one ($\bar{q}$). Each tangent direction is defined by an auxiliary vector $\mathbf{t}_q$, obtained by projecting $\mathbf{w}$ onto the respective hyperplane. Specifically, for each $q \in \{1, \ldots, Q\} \setminus \{\bar{q}\}$, $\mathbf{t}_q$ is given by

$$\mathbf{t}_q = \left(\mathbf{I} - \mathbf{n}_q \mathbf{n}_q^\top \right) \mathbf{w} + \boldsymbol{\epsilon} \chi \left(\left\| \left(\mathbf{I} - \mathbf{n}_q \mathbf{n}_q^\top \right) \mathbf{w} \right\| \right), \tag{31}$$

where $\chi : \mathbb{R} \to \{0, 1\}$ is an indicator function with $\chi(0) = 1$ and $\chi(s) = 0$ when $s \neq 0$, and the vector $\boldsymbol{\epsilon} \neq \mathbf{0}$ is such that $\mathbf{w}^\top \boldsymbol{\epsilon} = 0$. The first term in (31) is the projection of $\mathbf{w}$ onto the hyperplane defined by the normal vector $\mathbf{n}_q$, and the second term guarantees decisiveness when $\mathbf{n}_q = -\mathbf{w}$.

Except where otherwise noted, content of this paper is licensed under a Creative Commons Attribution 4.0 International License.

The reproduction and distribution with attribution of the entire paper or of individual pages, in electronic or printed form, including any material under non-CC-BY 4.0 licenses is hereby granted by the authors and respective copyright owners.

Consider now a hybrid mode defined by $\boldsymbol{\xi} = (\hat{\mathbf{p}}, q)$, where the conditions in (27) and (28) are satisfied. At the next jump, we assess whether the safe half-space $\hat{q}$ contains $\bar{\mathbf{p}}$. If it does, the next setpoint is simply set to $\bar{\mathbf{p}}$. When the safe half-space $\hat{q}$ does not contain $\bar{\mathbf{p}}$, we proceed as follows. First, we determine the point $\tilde{\mathbf{p}}$ where the boundary hyperplane $\hat{q}$ intersects the line segment between the current position $\mathbf{p}$ and $\bar{\mathbf{p}}$. We then adjust $\tilde{\mathbf{p}}$ by adding $\mathbf{t}_{\hat{q}}$ scaled by a factor $\tau \in \mathbb{R}_{\geq 0}$, resulting in the new setpoint. The factor τ is the smallest nonnegative value that ensures the new setpoint satisfies the synergy gap condition.

More specifically, the active target point is updated according to

$$\hat{\mathbf{p}}^{+} = \begin{cases} \tilde{\mathbf{p}} + \mathbf{t}_{\hat{q}}\tau, & \text{if } h_{\hat{q}}(\bar{\mathbf{p}}) < 0 \text{ and } (\mathbf{p}, \boldsymbol{\xi}) \in \mathcal{J}, \\ \bar{\mathbf{p}}, & \text{if } h_{\hat{q}}(\bar{\mathbf{p}}) \geq 0 \text{ and } (\mathbf{p}, \boldsymbol{\xi}) \in \mathcal{J}, \end{cases} \tag{32}$$

where $\tilde{\mathbf{p}}$ is the intersection point between the line segment $\overline{\mathbf{p}\bar{\mathbf{p}}}$ and the boundary hyperplane $\hat{q}$, given by

$$\tilde{\mathbf{p}} = \mathbf{p} + \frac{h_{\hat{q}}(\mathbf{p})}{h_{\hat{q}}(\mathbf{p}) - h_{\hat{q}}(\bar{\mathbf{p}})}(\bar{\mathbf{p}} - \mathbf{p}), \tag{33}$$

and the scaling factor $\tau \in \mathbb{R}_{\geq 0}$ is determined as follows:

$$\begin{aligned} \tau = \min_{(\tau', q') \in \mathbb{R}_{\geq 0} \times \hat{\mathcal{Q}}_{\hat{q}}} \quad & \tau' \\ \text{subject to } & h_{q'}\left(\tilde{\mathbf{p}} + \mathbf{t}_{\hat{q}}\tau'\right) \geq \mu. \end{aligned} \tag{34}$$

The optimization problem in (34) can be compactly written as

$$\tau = \min_{q' \in \hat{\mathcal{Q}}_{\hat{q}}} \tau_{q'}, \tag{35}$$

where, for each $q' \in \hat{\mathcal{Q}}_{\hat{q}}$, $\tau_{q'}$ is given by

$$\tau_{q'} = \begin{cases} \left(\mathbf{n}_{q'}^{\top}\mathbf{t}_{\hat{q}}\right)^{-1}\left(\mu - h_{q'}(\tilde{\mathbf{p}})\right), & \text{if } h_{q'}(\tilde{\mathbf{p}}) < \mu \text{ and } \mathbf{n}_{q'}^{\top}\mathbf{t}_{\hat{q}} > 0, \\ 0, & \text{if } h_{q'}(\tilde{\mathbf{p}}) \geq \mu, \\ \infty \text{ (infeasible)}, & \text{otherwise.} \end{cases} \tag{36}$$

Note that when the safe half-space $\hat{q}$ does not contain $\bar{\mathbf{p}}$, the next setpoint is placed on the boundary hyperplane $\hat{q}$, and τ ensures that the next setpoint satisfies the synergy gap condition. Thus, if the current hybrid mode satisfies the conditions in (27) and (28), the update from (30) and (32) ensures that the next mode also satisfies these conditions when $h_{\hat{q}}(\bar{\mathbf{p}}) < 0$. The proposed switching logic is depicted in Fig. 2.

It now only remains to ensure that the initial hybrid mode satisfies the conditions in (27) and (28) when the initial active safe half-space does not contain $\bar{\mathbf{p}}$. To address this, the initial auxiliary state $\boldsymbol{\xi}_0 = (\hat{\mathbf{p}}_0, q_0)$ is computed through a pre-initial update. Specifically, the active safe half-space is initialized through

$$q_0 = \arg\max_{q' \in \{1,\ldots,Q\}} h_{q'}(\mathbf{p}_0), \tag{37}$$

and the initial target point is determined according to

$$\hat{\mathbf{p}}_0 = \begin{cases} \tilde{\mathbf{p}}_0 + \mathbf{t}_{q_0}\tau_0, & \text{if } h_{q_0}(\bar{\mathbf{p}}) < 0, \\ \bar{\mathbf{p}}, & \text{if } h_{q_0}(\bar{\mathbf{p}}) \geq 0, \end{cases} \tag{38}$$

where $\tilde{\mathbf{p}}_0$ is the intersection point of $\overline{\mathbf{p}_0\bar{\mathbf{p}}}$ with the hyperplane q_0, and τ_0 is given by (35) ($\hat{q} = q_0$, $\tilde{\mathbf{p}} = \tilde{\mathbf{p}}_0$).

Except where otherwise noted, content of this paper is licensed under a Creative Commons Attribution 4.0 International License.

The reproduction and distribution with attribution of the entire paper or of individual pages, in electronic or printed form, including any material under non-CC-BY 4.0 licenses is hereby granted by the authors and respective copyright owners.

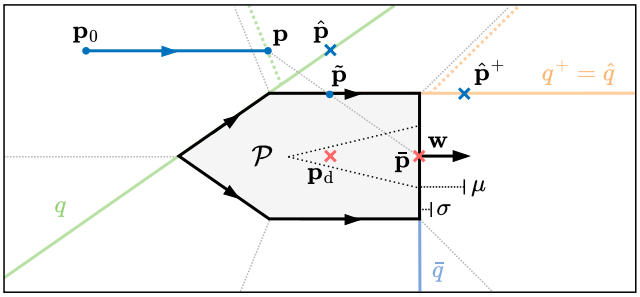

Fig. 2 Illustration of the switching mechanism triggered by a jump event when the forecast safe half-space $\hat{q}$ does not contain the desired rendezvous point $\bar{\mathbf{p}}$.

Finally, once the chaser spacecraft enters a neighborhood of the rendezvous point $\bar{\mathbf{p}}$, the algorithm transitions into the docking mode. In this phase, the active controller becomes $\mathbf{k}_{\mathrm{d},1}$, which guides the spacecraft toward the target docking location $\bar{\mathbf{p}}_\mathrm{d}$ while ensuring it remains within the set $\mathcal{D}$. With the proposed switching mechanism now fully outlined, Algorithm 1 summarizes the hybrid control strategy, highlighting its computational implementation. We are now ready to present the main result of this paper.

Theorem 3 *Consider the dynamics* (11)-(12). *If there exists a controller* $\mathbf{k}_{\boldsymbol{\xi},1} : \mathbb{R}^p \times \mathbb{R}^p \to \mathbb{R}^m$ *that solves the safe stabilization subproblem defined by* $\boldsymbol{\xi} = (\hat{\mathbf{p}}, q) \in \Xi$, *and there exists a controller* $\mathbf{k}_{\mathrm{d},1} : \mathbb{R}^p \times \mathbb{R}^p \to \mathbb{R}^m$ *that solves the docking subproblem, then, for every initial condition* $(\mathbf{p}_0, \mathbf{v}_0) \in \mathrm{int}(C) \times \mathbb{R}^p$, *the hybrid control strategy described in this section guarantees that the resulting chaser trajectory* $\boldsymbol{\varphi} : \mathbb{R}_{\geq 0} \to \mathbb{R}^p$ *satisfies* $\lim_{t\to\infty} \|\boldsymbol{\varphi}(t) - \mathbf{p}_\mathrm{d}\| = 0$ *and* $\boldsymbol{\varphi}(t) \in C$ *for all* $t \in \mathbb{R}_{\geq 0}$.

Proof *According to [37],* $\boldsymbol{\varphi}$ *will first converge to* $\bar{\mathbf{p}}$. *Since, by design, the ball defined by* $\|\mathbf{p} - \bar{\mathbf{p}}\| \leq r$ *lies entirely within* $\mathrm{int}(\mathcal{D})$, *there exists an instant at which the algorithm transitions to the docking mode. In this phase, the controller* $\mathbf{k}_{\mathrm{d},1}$ *safely drives the spacecraft to* $\mathbf{p}_\mathrm{d}$, *completing the proof.*

Algorithm 1 Hybrid Control Algorithm

Require: $\mathbf{p}_0$, $\mathbf{v}_0$, $\bar{\mathbf{p}}$, $h_1, \ldots, h_Q$, μ, σ, r, $\mathbf{k}_{\boldsymbol{\xi},1}$, $\mathbf{k}_{\mathrm{d},1}$

Compute $\mathbf{w}$ using (23)-(24) ▷ Setup
Initialize $\boldsymbol{\xi} = (\hat{\mathbf{p}}, q)$ using (37)-(38)
Initialize $\hat{q}$ using (25)-(26)
while $\|\mathbf{p} - \bar{\mathbf{p}}\| > r$ **do** ▷ Rendezvous Phase
    Get current state $(\mathbf{p}, \mathbf{v})$ and time t
    if $h_{\hat{q}}(\mathbf{p}) - h_q(\mathbf{p}) \geq \sigma$ and $h_q(\mathbf{p}) \geq 0$ **then** ▷ Jump Event
        if $h_{\hat{q}}(\bar{\mathbf{p}}) < 0$ **then**
            Compute $\tilde{\mathbf{p}}$, $\mathbf{t}_{\hat{q}}$, τ via (33), (31), (35)-(36)
            $(\hat{\mathbf{p}}, q) \leftarrow (\tilde{\mathbf{p}} + \mathbf{t}_{\hat{q}}\tau, \hat{q})$
        else
            $(\hat{\mathbf{p}}, q) \leftarrow (\bar{\mathbf{p}}, \hat{q})$
        end if
        Update $\hat{q}$ using (25)-(26)
    end if
    Apply input $\mathbf{k}_{\boldsymbol{\xi},1}(\mathbf{p}, \mathbf{v}, t)$ to the spacecraft
end while
while true **do** ▷ Docking Phase
    Get current state $(\mathbf{p}, \mathbf{v})$ and time t
    Apply input $\mathbf{k}_{\mathrm{d},1}(\mathbf{p}, \mathbf{v}, t)$ to the spacecraft
end while

Except where otherwise noted, content of this paper is licensed under a Creative Commons Attribution 4.0 International License.

The reproduction and distribution with attribution of the entire paper or of individual pages, in electronic or printed form, including any material under non-CC-BY 4.0 licenses is hereby granted by the authors and respective copyright owners.

4.2 Controller Design - Rendezvous

To complete the description of the hybrid control strategy for the rendezvous phase, it now remains to address the design of the controller $\mathbf{k}_{\boldsymbol{\xi},1}$, which must solve the safe stabilization subproblem associated with the auxiliary state $\boldsymbol{\xi} = (\hat{\mathbf{p}}, q) \in \Xi$. Following [37], the design of $\mathbf{k}_{\boldsymbol{\xi},1}$ proceeds in two stages. First, we design a smooth CLF-CBF controller $\mathbf{k}_{\boldsymbol{\xi}} : \mathbb{R}^p \to \mathbb{R}^p$ for the top-level dynamics (11) under compatible CLF and CBF constraints. Next, we follow a joint CLF-CBF backstepping approach to obtain compatible CLF and CBF constraints for the full dynamics (11)-(12), which are used to design $\mathbf{k}_{\boldsymbol{\xi},1}$ through a QP.

Regarding the first design step, we consider a quadratic CLF $V_{\hat{\mathbf{p}}} : \mathbb{R}^p \to \mathbb{R}_{\geq 0}$ for (11), defined as

$$V_{\hat{\mathbf{p}}}(\mathbf{p}) = \frac{1}{2}\|\mathbf{p} - \hat{\mathbf{p}}\|^2 \tag{39}$$

for all $\mathbf{p} \in \mathbb{R}^p$, along with the CBF h_q defined by (15). As the top-level dynamics (11) are fully actuated, these functions are a valid CLF and CBF for (11), and the associated constraints take the form

$$\begin{aligned} \nabla V_{\hat{\mathbf{p}}}(\mathbf{p})^\top \mathbf{v} &\leq -\gamma\left(V_{\hat{\mathbf{p}}}(\mathbf{p})\right), \\ \nabla h_q(\mathbf{p})^\top \mathbf{v} &\geq -\alpha\left(h_q(\mathbf{p})\right), \end{aligned} \tag{40}$$

where the class-$\mathcal{K}$ function γ (for the CLF) and the extended class-$\mathcal{K}_\infty$ function α (for the CBF) can be chosen arbitrarily. For simplicity, we select $\gamma(s) = 2\bar{\gamma}s$ for all $s \in \mathbb{R}_{\geq 0}$ and $\alpha(s) = \bar{\alpha}s$ for all $s \in \mathbb{R}$, with $\bar{\gamma}, \bar{\alpha} \in \mathbb{R}_{>0}$. As shown in [37], choosing $\bar{\alpha} \geq \bar{\gamma}$ ensures that the CLF and CBF constraints are compatible (mutually satisfiable for all $\mathbf{p} \in \mathbb{R}^p$), allowing synthesis of a top-level controller $\mathbf{k}_{\boldsymbol{\xi}}$ without relaxing the stabilization objective. However, since the top-level controller must be smooth, QP-based synthesis is not suitable, as QP controllers are typically only locally Lipschitz. To achieve smoothness while satisfying both constraints, we employ the Gaussian-weighted centroid method introduced in [44]. For brevity, the details of the method are omitted here, but the reader is referred to [44] and [37] for a full description.

Having obtained the top-level controller $\mathbf{k}_{\boldsymbol{\xi}}$, we can now construct a CLF $V_{\hat{\mathbf{p}},1} : \mathbb{R}^p \times \mathbb{R}^p \to \mathbb{R}_{\geq 0}$ and a CBF $h_{q,1} : \mathbb{R}^p \times \mathbb{R}^p \to \mathbb{R}$ for the overall spacecraft dynamics (11)-(12) as

$$\begin{aligned} V_{\hat{\mathbf{p}},1}(\mathbf{p}, \mathbf{v}) &= V_{\hat{\mathbf{p}}}(\mathbf{p}) + \frac{1}{2\beta_v}\left\|\mathbf{v} - \mathbf{k}_{\boldsymbol{\xi}}(\mathbf{p})\right\|^2, \\ h_{q,1}(\mathbf{p}, \mathbf{v}) &= h_q(\mathbf{p}) - \frac{1}{2\beta_h}\left\|\mathbf{v} - \mathbf{k}_{\boldsymbol{\xi}}(\mathbf{p})\right\|^2, \end{aligned} \tag{41}$$

for all $(\mathbf{p}, \mathbf{v}) \in \mathbb{R}^p \times \mathbb{R}^p$, with $\beta_v, \beta_h \in \mathbb{R}_{>0}$. As the overall dynamics (11)-(12) are fully actuated, these functions are a valid CLF and CBF for (11)-(12), and the associated constraints take the form

$$\begin{aligned} \left(L_{\bar{\mathbf{f}}_1} V_{\hat{\mathbf{p}},1}\right)(\mathbf{p}, \mathbf{v}, t) + \left(L_{\bar{\mathbf{G}}_1} V_{\hat{\mathbf{p}},1}\right)(\mathbf{p}, \mathbf{v}, t)\mathbf{u} &\leq -\gamma_1\left(V_{\hat{\mathbf{p}},1}(\mathbf{p}, \mathbf{v})\right), \\ \left(L_{\bar{\mathbf{f}}_1} h_{q,1}\right)(\mathbf{p}, \mathbf{v}, t) + \left(L_{\bar{\mathbf{G}}_1} h_{q,1}\right)(\mathbf{p}, \mathbf{v}, t)\mathbf{u} &\geq -\alpha_1\left(h_{q,1}(\mathbf{p}, \mathbf{v})\right), \end{aligned} \tag{42}$$

where the fields $\bar{\mathbf{f}}_1$ and $\bar{\mathbf{G}}_1$ are defined as $\bar{\mathbf{f}}_1(\mathbf{p}, \mathbf{v}, t) = (\mathbf{v}, \mathbf{f}_1(\mathbf{p}, \mathbf{v}, t))$ and $\bar{\mathbf{G}}_1(\mathbf{p}, \mathbf{v}, t) = [\mathbf{0}^\top \mathbf{G}_1(\mathbf{p}, \mathbf{v}, t)^\top]^\top$, γ_1 is a class-$\mathcal{K}$ function with $\gamma_1(s) < \gamma(s)$ for all $s \in \mathbb{R}_{>0}$, and α_1 is an extended class-$\mathcal{K}_\infty$ function such that $\alpha_1(s) \geq \alpha(s)$ for all $s \in \mathbb{R}$. By virtue of the joint CLF-CBF backstepping design, these constraints are compatible, as established in [45] and [37].

Remark 2 (Maintaining Safety across Jumps) *To maintain safety when an update occurs, the state* $(\mathbf{p}, \mathbf{v})$ *at the moment of the jump must satisfy* $h_{q^+,1}(\mathbf{p}, \mathbf{v}) \geq 0$. *As shown in Section 4, the position* $\mathbf{p}$ *will be within the interior of the next active safe half-space, so that* $h_{q^+}(\mathbf{p}) > 0$ *at the time of the jump. Hence, we can select the gain* β_h *such that* $h_{q^+,1}(\mathbf{p}, \mathbf{v}) \geq 0$ *to preserve safety across transitions. This means that in practice, the value of* β_h *may have to change when a jump occurs. However, for simplicity of notation,*

Except where otherwise noted, content of this paper is licensed under a Creative Commons Attribution 4.0 International License.

The reproduction and distribution with attribution of the entire paper or of individual pages, in electronic or printed form, including any material under non-CC-BY 4.0 licenses is hereby granted by the authors and respective copyright owners.

this parameter dependence has been omitted. Given a nominal value $\bar{\beta}_h$, we can then update β_h as

$$\beta_h^+ = \max\left\{\bar{\beta}_h, \frac{1}{2h_{q^+}(\mathbf{p})}\left\|\mathbf{v} - \mathbf{k}_{\boldsymbol{\xi}^+}(\mathbf{p})\right\|^2\right\}. \tag{43}$$

Given the compatible CLF and CBF constraints in (42) and assuming an unbounded control input, we can then construct an optimization-based controller $\mathbf{k}_{\boldsymbol{\xi},1}$ as follows:

$$\begin{aligned}\mathbf{k}_{\boldsymbol{\xi},1}(\mathbf{p},\mathbf{v},t) = \underset{\mathbf{u}\in\mathbb{R}^m}{\arg\min}\ & \frac{1}{2}\|\mathbf{u} - \mathbf{k}_{\mathrm{n}}(\mathbf{p},\mathbf{v},t)\|^2 \\ \text{subject to}\ & \left(L_{\bar{\mathbf{f}}_1}V_{\hat{\mathbf{p}},1}\right)(\mathbf{p},\mathbf{v},t) + \left(L_{\bar{\mathbf{G}}_1}V_{\hat{\mathbf{p}},1}\right)(\mathbf{p},\mathbf{v},t)\mathbf{u} \le -\gamma_1\left(V_{\hat{\mathbf{p}},1}(\mathbf{p},\mathbf{v})\right), \\ & \left(L_{\bar{\mathbf{f}}_1}h_{q,1}\right)(\mathbf{p},\mathbf{v},t) + \left(L_{\bar{\mathbf{G}}_1}h_{q,1}\right)(\mathbf{p},\mathbf{v},t)\mathbf{u} \ge -\alpha_1\left(h_{q,1}(\mathbf{p},\mathbf{v})\right),\end{aligned} \tag{44}$$

which solves the subproblem corresponding to $\boldsymbol{\xi} = (\hat{\mathbf{p}}, q) \in \Xi$. To account for input bounds of the form $\|\mathbf{u}\| \le u_{\max}$, with $u_{\max} \in \mathbb{R}_{>0}$, the CLF constraint must be relaxed, which can be done by introducing a relaxation function $\delta_{\boldsymbol{\xi}} : \mathbb{R}^p \times \mathbb{R}^p \times \mathbb{R}_{\ge 0} \to \mathbb{R}_{\ge 0}$. In this setting, the "best effort" we can do to achieve the stabilization goal is to relax the CLF constraint only as much as necessary to ensure that the respective control half-space intersects the admissible input set. This corresponds to defining $\delta_{\boldsymbol{\xi}}$ as

$$\delta_{\boldsymbol{\xi}}(\mathbf{p},\mathbf{v},t) = \max\left\{0, \left(L_{\bar{\mathbf{f}}_1}V_{\hat{\mathbf{p}},1}\right)(\mathbf{p},\mathbf{v},t) + \gamma_1\left(V_{\hat{\mathbf{p}},1}(\mathbf{p},\mathbf{v})\right) - \left\|\left(L_{\bar{\mathbf{G}}_1}V_{\hat{\mathbf{p}},1}\right)(\mathbf{p},\mathbf{v},t)\right\| u_{\max}\right\}. \tag{45}$$

Then, to incorporate the safety objective, we can adopt the optimal-decay QP formulation introduced in [42], which leads to the following subproblem controller design:

$$\begin{aligned}\left(\mathbf{k}_{\boldsymbol{\xi},1}(\mathbf{p},\mathbf{v},t),\cdot\right) = \underset{(\mathbf{u},\omega)\in\mathbb{R}^{m+1}}{\arg\min}\ & \frac{1}{2}\|\mathbf{u} - \mathbf{k}_{\mathrm{n}}(\mathbf{p},\mathbf{v},t)\|^2 + \frac{1}{2}p_\omega(\omega-1)^2 \\ \text{subject to}\ & \left(L_{\bar{\mathbf{f}}_1}V_{\hat{\mathbf{p}},1}\right)(\mathbf{p},\mathbf{v},t) + \left(L_{\bar{\mathbf{G}}_1}V_{\hat{\mathbf{p}},1}\right)(\mathbf{p},\mathbf{v},t)\mathbf{u} \le -\gamma_1\left(V_{\hat{\mathbf{p}},1}(\mathbf{p},\mathbf{v})\right) + \delta_{\boldsymbol{\xi}}(\mathbf{p},\mathbf{v},t), \\ & \left(L_{\bar{\mathbf{f}}_1}h_{q,1}\right)(\mathbf{p},\mathbf{v},t) + \left(L_{\bar{\mathbf{G}}_1}h_{q,1}\right)(\mathbf{p},\mathbf{v},t)\mathbf{u} \ge -\omega\alpha_1\left(h_{q,1}(\mathbf{p},\mathbf{v})\right), \\ & \|\mathbf{u}\| \le u_{\max},\end{aligned} \tag{46}$$

with $p_\omega \in \mathbb{R}_{>0}$. This QP is feasible when $h_{q,1}(\mathbf{p},\mathbf{v}) > 0$, as the CLF constraint has been relaxed to respect the input bound and $\omega\alpha_1\left(h_{q,1}(\mathbf{p},\mathbf{v})\right)$ can take any value when $h_{q,1}(\mathbf{p},\mathbf{v}) > 0$. When $h_{q,1}(\mathbf{p},\mathbf{v}) = 0$, the CLF and CBF constraints remain compatible, and the CLF constraint respects the input bound; however, the three constraints may not always be jointly satisfiable because ω is ineffective when $h_{q,1}(\mathbf{p},\mathbf{v}) = 0$. Nonetheless, this potential infeasibility arises only due to the input bound, and if $u_{\max}$ is sufficiently large, the QP remains feasible when $h_{q,1}(\mathbf{p},\mathbf{v}) = 0$.

4.3 Controller Design - Docking

To complete the description of the hybrid control strategy, we now address the design of the controller $\mathbf{k}_{\mathrm{d},1}$, which must solve the safe stabilization subproblem concerning the docking phase. The design process of $\mathbf{k}_{\mathrm{d},1}$ parallels that of $\mathbf{k}_{\boldsymbol{\xi},1}$, i.e., we first construct a smooth CLF-CBF controller $\mathbf{k}_{\mathrm{d}} : \mathbb{R}^p \to \mathbb{R}^p$ for the top-level dynamics (11) under compatible CLF and CBF constraints (made feasible by the convexity of $\mathcal{D}$), and we then extend this design using a joint CLF-CBF backstepping procedure to derive compatible CLF and CBF constraints for the complete system dynamics (11)-(12).

Regarding the first design step, we consider a quadratic CLF $V_{\mathrm{d}} : \mathbb{R}^p \to \mathbb{R}_{\ge 0}$ for (11), defined as

$$V_{\mathrm{d}}(\mathbf{p}) = \frac{1}{2}\|\mathbf{p} - \mathbf{p}_{\mathrm{d}}\|^2 \tag{47}$$

for all $\mathbf{p} \in \mathbb{R}^p$. However, since $\mathcal{D}$ is the intersection of multiple half-spaces, we cannot directly obtain a

Except where otherwise noted, content of this paper is licensed under a Creative Commons Attribution 4.0 International License.

The reproduction and distribution with attribution of the entire paper or of individual pages, in electronic or printed form, including any material under non-CC-BY 4.0 licenses is hereby granted by the authors and respective copyright owners.

top-level CBF. To overcome this, we consider a smooth approximation of the minimum function, adopting the LogSumExp approach from [43]. More specifically, we define a CBF $h_\mathrm{d} : \mathbb{R}^p \to \mathbb{R}$ for (11) as

$$h_\mathrm{d}(\mathbf{p}) = -\frac{1}{\kappa} \ln \left(\sum_{i=1}^{M} \exp(-\kappa \psi_i(\mathbf{p})) \right) \tag{48}$$

for all $\mathbf{p} \in \mathbb{R}^p$, with tuning parameter $\kappa \in \mathbb{R}_{>0}$, which defines a safe set $\tilde{\mathcal{D}} \subseteq \mathcal{D}$ for the chaser position, such that $\lim_{\kappa \to \infty} \tilde{\mathcal{D}} = \mathcal{D}$. As the top-level dynamics (11) are fully actuated, these functions are a valid CLF and CBF for (11), and the associated constraints take the form

$$\begin{aligned} \nabla V_\mathrm{d}(\mathbf{p})^\top \mathbf{v} &\leq -\gamma(V_\mathrm{d}(\mathbf{p})), \\ \nabla h_\mathrm{d}(\mathbf{p})^\top \mathbf{v} &\geq -\alpha(h_\mathrm{d}(\mathbf{p})), \end{aligned} \tag{49}$$

where the class-$\mathcal{K}$ function γ and the extended class-$\mathcal{K}_\infty$ function α can be chosen arbitrarily.

As demonstrated in [37], the above constraints are compatible if it holds that

$$\alpha(h_\mathrm{d}(\mathbf{p})) \geq \frac{\|\nabla h_\mathrm{d}(\mathbf{p})\|}{\|\nabla V_\mathrm{d}(\mathbf{p})\|} \gamma\left(V_\mathrm{d}(\mathbf{p})\right) \tag{50}$$

for all $\mathbf{p}$ belonging to the critical set

$$\mathcal{S}_\mathrm{d}^\mathrm{c} = \left\{ \mathbf{p} \in \mathbb{R}^p : \frac{\nabla V_\mathrm{d}(\mathbf{p})}{\|\nabla V_\mathrm{d}(\mathbf{p})\|} = \frac{\nabla h_\mathrm{d}(\mathbf{p})}{\|\nabla h_\mathrm{d}(\mathbf{p})\|}, \nabla V_\mathrm{d}(\mathbf{p}) \neq \mathbf{0}, \nabla h_\mathrm{d}(\mathbf{p}) \neq \mathbf{0} \right\}. \tag{51}$$

For simplicity, we now consider that, due to the symmetry of the docking port and the location of the docking point, the critical set $\mathcal{S}_\mathrm{d}^\mathrm{c}$ reduces to an open ray given by

$$\mathcal{S}_\mathrm{d}^\mathrm{c} = \{ \mathbf{p}_\mathrm{d} + \mathbf{d}_\mathrm{c} \lambda : \lambda \in \mathbb{R}_{>0} \}, \tag{52}$$

with $\mathbf{d}_\mathrm{c} \in \mathbb{S}^{p-1}$, and $\psi_i(\mathbf{p}_\mathrm{d}) = \bar{\psi}_\mathrm{d} \in \mathbb{R}_{>0}$ for all $i \in \{1, \ldots, M\}$. Also, we again select $\gamma(s) = 2\bar{\gamma}s$ for all $s \in \mathbb{R}_{\geq 0}$ and $\alpha(s) = \bar{\alpha}s$ for all $s \in \mathbb{R}$, with $\bar{\gamma}, \bar{\alpha} \in \mathbb{R}_{>0}$. With these design choices, and using the bounds

$$\begin{aligned} h_\mathrm{d}(\mathbf{p}) &\geq \min_{i \in \{1,\ldots,M\}} \psi_i(\mathbf{p}) - \frac{\ln(M)}{\kappa}, \\ \|\nabla h_\mathrm{d}(\mathbf{p})\| &\leq 1, \end{aligned} \tag{53}$$

(see [43]), the compatibility of the top-level constraints can be achieved by ensuring that, for all $\lambda \in \mathbb{R}_{>0}$,

$$\begin{aligned} \bar{\alpha} \left(\min_{i \in \{1,\ldots,M\}} \psi_i(\mathbf{p}_\mathrm{d} + \mathbf{d}_\mathrm{c}\lambda) - \frac{\ln(M)}{\kappa} \right) \geq \frac{2\bar{\gamma} V_\mathrm{d}(\mathbf{p}_\mathrm{d} + \mathbf{d}_\mathrm{c}\lambda)}{\|\nabla V_\mathrm{d}(\mathbf{p}_\mathrm{d} + \mathbf{d}_\mathrm{c}\lambda)\|} \iff \\ \bar{\alpha} \left(\bar{\psi}_\mathrm{d} - \frac{\ln(M)}{\kappa} \right) + \min_{i \in \{1,\ldots,M\}} \left(\bar{\alpha} \mathbf{a}_i^\top \mathbf{d}_\mathrm{c} - \bar{\gamma} \right) \lambda \geq 0. \end{aligned} \tag{54}$$

This condition is satisfied by selecting the design parameters as

$$\begin{aligned} \kappa &\geq \frac{\ln(M)}{\bar{\psi}_\mathrm{d}}, \\ \bar{\alpha} &\geq \max_{i \in \{1,\ldots,M\}} \frac{\bar{\gamma}}{\mathbf{a}_i^\top \mathbf{d}_\mathrm{c}}. \end{aligned} \tag{55}$$

Having obtained compatible CLF and CBF constraints for (11), we can then design a smooth top-level controller $\mathbf{k}_\mathrm{d}$ using the Gaussian-weighted centroid method introduced in [44].

Except where otherwise noted, content of this paper is licensed under a Creative Commons Attribution 4.0 International License.

The reproduction and distribution with attribution of the entire paper or of individual pages, in electronic or printed form, including any material under non-CC-BY 4.0 licenses is hereby granted by the authors and respective copyright owners.

Having obtained the top-level controller $\mathbf{k}_{\mathrm{d}}$, we can now construct a CLF $V_{\mathrm{d},1} : \mathbb{R}^p \times \mathbb{R}^p \to \mathbb{R}_{\geq 0}$ and a CBF $h_{\mathrm{d},1} : \mathbb{R}^p \times \mathbb{R}^p \to \mathbb{R}$ for the overall spacecraft dynamics (11)-(12) as

$$\begin{aligned} V_{\mathrm{d},1}(\mathbf{p}, \mathbf{v}) &= V_{\mathrm{d}}(\mathbf{p}) + \frac{1}{2\beta_v}\|\mathbf{v} - \mathbf{k}_{\mathrm{d}}(\mathbf{p})\|^2, \\ h_{\mathrm{d},1}(\mathbf{p}, \mathbf{v}) &= h_{\mathrm{d}}(\mathbf{p}) - \frac{1}{2\beta_h}\|\mathbf{v} - \mathbf{k}_{\mathrm{d}}(\mathbf{p})\|^2, \end{aligned} \tag{56}$$

for all $(\mathbf{p}, \mathbf{v}) \in \mathbb{R}^p \times \mathbb{R}^p$, with $\beta_v, \beta_h \in \mathbb{R}_{>0}$. As the spacecraft dynamics (11)-(12) are fully actuated, these functions are a valid CLF and CBF for (11)-(12), and the associated constraints are compatible.

Remark 3 (Maintaining Safety across the Transition to Docking Mode) *To guarantee safety during the switch to docking mode, the system state* $(\mathbf{p}, \mathbf{v})$ *at the transition moment must satisfy* $h_{\mathrm{d},1}(\mathbf{p}, \mathbf{v}) \geq 0$. *By design, we have* $\psi_i(\mathbf{p}) > 0$ *for all* $i \in \{1, \ldots, M\}$, *which allows us to choose* κ *such that* $h_{\mathrm{d}}(\mathbf{p}) > 0$ *at the transition moment. Consequently,* β_h *can then be selected using the same process from* (43).

Assuming an unbounded input, we can then design an optimization-based controller $\mathbf{k}_{\mathrm{d},1}$ as follows:

$$\begin{aligned} \mathbf{k}_{\mathrm{d},1}(\mathbf{p}, \mathbf{v}, t) = \underset{\mathbf{u} \in \mathbb{R}^m}{\arg\min}\ & \frac{1}{2}\|\mathbf{u} - \mathbf{k}_{\mathrm{n}}(\mathbf{p}, \mathbf{v}, t)\|^2 \\ \text{subject to } & \left(L_{\bar{\mathbf{f}}_1} V_{\mathrm{d},1}\right)(\mathbf{p}, \mathbf{v}, t) + \left(L_{\bar{\mathbf{G}}_1} V_{\mathrm{d},1}\right)(\mathbf{p}, \mathbf{v}, t)\mathbf{u} \leq -\gamma_1\left(V_{\mathrm{d},1}(\mathbf{p}, \mathbf{v})\right), \\ & \left(L_{\bar{\mathbf{f}}_1} h_{\mathrm{d},1}\right)(\mathbf{p}, \mathbf{v}, t) + \left(L_{\bar{\mathbf{G}}_1} h_{\mathrm{d},1}\right)(\mathbf{p}, \mathbf{v}, t)\mathbf{u} \geq -\alpha_1\left(h_{\mathrm{d},1}(\mathbf{p}, \mathbf{v})\right), \end{aligned} \tag{57}$$

which solves the docking subproblem. To account for bounded inputs, we follow the same approach from the previous subsection, which leads to the following subproblem controller design:

$$\begin{aligned} (\mathbf{k}_{\mathrm{d},1}(\mathbf{p}, \mathbf{v}, t), \cdot) = \underset{(\mathbf{u}, \omega) \in \mathbb{R}^{m+1}}{\arg\min}\ & \frac{1}{2}\|\mathbf{u} - \mathbf{k}_{\mathrm{n}}(\mathbf{p}, \mathbf{v}, t)\|^2 + \frac{1}{2}p_\omega(\omega - 1)^2 \\ \text{subject to } & \left(L_{\bar{\mathbf{f}}_1} V_{\mathrm{d},1}\right)(\mathbf{p}, \mathbf{v}, t) + \left(L_{\bar{\mathbf{G}}_1} V_{\mathrm{d},1}\right)(\mathbf{p}, \mathbf{v}, t)\mathbf{u} \leq -\gamma_1\left(V_{\mathrm{d},1}(\mathbf{p}, \mathbf{v})\right) + \delta_{\mathrm{d}}(\mathbf{p}, \mathbf{v}, t), \\ & \left(L_{\bar{\mathbf{f}}_1} h_{\mathrm{d},1}\right)(\mathbf{p}, \mathbf{v}, t) + \left(L_{\bar{\mathbf{G}}_1} h_{\mathrm{d},1}\right)(\mathbf{p}, \mathbf{v}, t)\mathbf{u} \geq -\alpha_1\left(h_{\mathrm{d},1}(\mathbf{p}, \mathbf{v})\right), \\ & \|\mathbf{u}\| \leq u_{\max}. \end{aligned} \tag{58}$$

5 Simulation Results

This section demonstrates the effectiveness of the proposed hybrid CLF-CBF control strategy in a realistic spacecraft rendezvous and docking setting. The target spacecraft is considered to be in a circular orbit around the Earth, and the gravitational pull caused by the spacecraft is assumed to be negligible. For simplicity, the motion of the spacecraft is restricted to the orbital plane, and the dynamics are expressed using the Earth-Centered Inertial (ECI) and Local Vertical Local Horizontal (LVLH) frames. The ECI frame has its origin at the center of the Earth and is nonrotating. Conversely, the LVLH frame (target-fixed frame) is fixed to the body of the target spacecraft, with its origin at the center of the target, and its axes are defined as follows: the z-axis points from the target to the center of the Earth, and the x-axis has the direction of the velocity of the target, similar to the scenario from Fig. 1. Under this configuration, the chaser dynamics in the LVLH frame are described by

$$\begin{aligned} \dot{\mathbf{p}} &= \mathbf{v}, \\ \dot{\mathbf{v}} &= -\mathbf{S}(\omega)^2\mathbf{p} - 2\mathbf{S}(\omega)\mathbf{v} - \omega^2 R_{\mathrm{T}}\mathbf{e}_2 - \frac{G m_{\mathrm{E}}}{\|\mathbf{R}(t)\mathbf{p} + \boldsymbol{\varphi}_{\mathrm{T}}(t)\|^3}\left(\mathbf{p} + \mathbf{R}(t)^\top \boldsymbol{\varphi}_{\mathrm{T}}(t)\right) + \frac{1}{m_{\mathrm{C}}}\mathbf{u}, \end{aligned} \tag{59}$$

where $\mathbf{p}, \mathbf{v} \in \mathbb{R}^2$ denote the position and velocity of the chaser in the LVLH frame, respectively, G is the

Except where otherwise noted, content of this paper is licensed under a Creative Commons Attribution 4.0 International License.

The reproduction and distribution with attribution of the entire paper or of individual pages, in electronic or printed form, including any material under non-CC-BY 4.0 licenses is hereby granted by the authors and respective copyright owners.

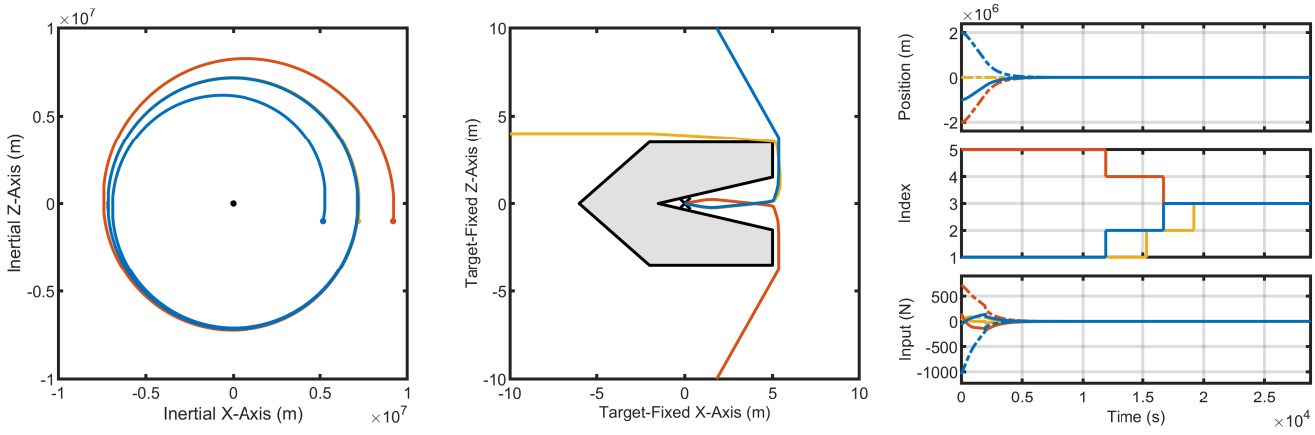

Fig. 3 Resulting trajectories and time profiles of the chaser spacecraft under the proposed hybrid control strategy for three initial positions and a given geometry of the target. The plots on the right display the respective time evolution of the position, the input, and the index of the active half-space for each trajectory. In the position and input plots, solid lines represent the first component and dotted lines the second.

Table 1 Main simulation parameters

Parameter	Value	Description
G	$6.674 \times 10^{-11}\,\mathrm{m^3\,kg^{-1}\,s^{-2}}$	Gravitational constant
m_E	$5.972 \times 10^{24}\,\mathrm{kg}$	Mass of the Earth
m_C	$100\,\mathrm{kg}$	Mass of the chaser
R_T	$7.171 \times 10^{6}\,\mathrm{m}$	Orbital radius of the target
u_max	$1500\,\mathrm{N}$	Input bound of the chaser
$\mathbf{p}_0$	$(-1\,\mathrm{Mm}, 2\,\mathrm{Mm})$; $(-1\,\mathrm{Mm}, 0)$; $(-1\,\mathrm{Mm}, -2\,\mathrm{Mm})$	Initial position of the chaser (LVLH)
$\mathbf{v}_0$	(0, 0); (0, 0); (0, 0)	Initial velocity of the chaser (LVLH)
μ	0.5	Minimum synergy gap
σ	0.1	Hysteresis width

gravitational constant, m_E is the mass of the Earth, m_C is the mass of the chaser, $R_\mathrm{T} \in \mathbb{R}_{>0}$ is the orbital radius of the target, $\omega = \sqrt{G m_\mathrm{E} R^{-3}}$ is the angular velocity of the LVLH frame relative to the ECI frame,

$$\mathbf{S}(\omega) = \begin{bmatrix} 0 & -\omega \\ \omega & 0 \end{bmatrix}, \tag{60}$$

and $\mathbf{u} \in \mathbb{R}^2$ denotes the control input (actuation force) acting on the chaser, expressed in the LVLH frame. Moreover, $\boldsymbol{\varphi}_\mathrm{T} : \mathbb{R}_{\geq 0} \to \mathbb{R}^2$ is the trajectory of the target (center) in the ECI frame, and $\mathbf{R} : \mathbb{R}_{\geq 0} \to \mathrm{SO}(2)$ outputs the rotation matrix from the LVLH to the ECI frame. These two functions are given by

$$\begin{aligned} \boldsymbol{\varphi}_\mathrm{T}(t) &= R_\mathrm{T}(\cos(\omega t), \sin(\omega t)), \\ \mathbf{R}(t) &= \begin{bmatrix} -\sin(\omega t) & -\cos(\omega t) \\ \cos(\omega t) & -\sin(\omega t) \end{bmatrix}. \end{aligned} \tag{61}$$

Fig. 3 presents the resulting trajectories and corresponding time profiles of the chaser spacecraft under the proposed hybrid control strategy for three distinct initial positions and a fixed geometry of the

Except where otherwise noted, content of this paper is licensed under a Creative Commons Attribution 4.0 International License.

The reproduction and distribution with attribution of the entire paper or of individual pages, in electronic or printed form, including any material under non-CC-BY 4.0 licenses is hereby granted by the authors and respective copyright owners.

target. The main simulation parameters are based on those in [13] and are summarized in Table 1. The nominal controller used in the simulations is defined as

$$\mathbf{k}_{\mathrm{n}}(\mathbf{p},\mathbf{v},t) = m_{\mathrm{C}}\mathbf{S}(\omega)^2\mathbf{p} + 2m_{\mathrm{C}}\mathbf{S}(\omega)\mathbf{v} + m_{\mathrm{C}}\omega^2 R_{\mathrm{T}}\mathbf{e}_2 + \frac{Gm_{\mathrm{E}}m_{\mathrm{C}}}{\|\mathbf{R}(t)\mathbf{p}+\boldsymbol{\varphi}_{\mathrm{T}}(t)\|^3}\left(\mathbf{p}+\mathbf{R}(t)^\top\boldsymbol{\varphi}_{\mathrm{T}}(t)\right), \tag{62}$$

which means that the acceleration of the chaser in the LVLH frame is being minimized. As shown in Fig. 3, the chaser successfully avoids colliding with the target and converges to the desired docking point in all cases. For the initial condition $\mathbf{p}_0 = (-1\,\mathrm{Mm}, 0)$, two valid choices exist for the initial active safe half-space, and the resulting trajectory depends on the initialization (here, it led the chaser to approach the docking point by passing above the target (depicted in yellow)).

6 Conclusion

This paper presented a hybrid CLF-CBF control strategy for safe spacecraft rendezvous and docking with a target spacecraft, whose geometry is modeled as a bounded nonconvex polytope. By integrating hybrid feedback logic with CLF-CBF-based design, the proposed approach guarantees safe global convergence to the docking point, effectively avoiding deadlocks that typically arise in standard CLF-CBF-QP formulations. The approach extends previous hybrid CLF-CBF frameworks to handle nonconvex obstacles and time-varying dynamics. Simulation results in a high-fidelity rendezvous and docking scenario confirmed the effectiveness of the proposed control strategy under practical mission conditions.

Acknowledgments

This research was supported in part by CTS and LASI under grant CTS UID/00066/2025, and by project (1801P.01521.1.01) gEICko-101223148-IST-ID at ISR.

Declaration of Use of Artificial Intelligence

Artificial intelligence was not used in the work presented.

References

[1] Christophe Bonnal, Jean-Marc Ruault, and Marie-Christine Desjean. Active debris removal: Recent progress and current trends. *Acta Astronautica*, 85:51–60, 2013.

[2] Dale Arney, Richard Sutherland, John Mulvaney, Devon Steinkoenig, Christopher Stockdale, and Mason Farley. On-orbit servicing, assembly, and manufacturing (osam) state of play. 2021.

[3] Daniel Silvestre and Pedro Lourenço. Guidance and control for in-orbit servicing and assembly missions. In *Encyclopedia of Systems and Control Engineering*, pages 404–422. Elsevier, Oxford, first edition, 2026.

[4] Dennis Stone, Alan Lindenmoyer, George French, Elon Musk, David Gump, Chirinjeev Kathuria, Charles Miller, Mark Sirangelo, and Tom Pickens. Nasa's approach to commercial cargo and crew transportation. *Acta Astronautica*, 63(1-4):192–197, 2008.

[5] Ismael Lopez and Colin R Mclnnes. Autonomous rendezvous using artificial potential function guidance. *Journal of Guidance, Control, and Dynamics*, 18(2):237–241, 1995.

[6] Hongyang Dong, Qinglei Hu, and Maruthi R Akella. Safety control for spacecraft autonomous rendezvous and docking under motion constraints. *Journal of Guidance, Control, and Dynamics*, 40(7):1680–1692, 2017.

Except where otherwise noted, content of this paper is licensed under a Creative Commons Attribution 4.0 International License.

The reproduction and distribution with attribution of the entire paper or of individual pages, in electronic or printed form, including any material under non-CC-BY 4.0 licenses is hereby granted by the authors and respective copyright owners.

[7] Hongyang Dong, Qinglei Hu, and Maruthi R Akella. Dual-quaternion-based spacecraft autonomous rendezvous and docking under six-degree-of-freedom motion constraints. *Journal of Guidance, Control, and Dynamics*, 41(5):1150–1162, 2018.

[8] Richard Zappulla, Hyeongjun Park, Josep Virgili-Llop, and Marcello Romano. Real-time autonomous spacecraft proximity maneuvers and docking using an adaptive artificial potential field approach. *IEEE Transactions on Control Systems Technology*, 27(6):2598–2605, 2018.

[9] Yoram Koren, Johann Borenstein, et al. Potential field methods and their inherent limitations for mobile robot navigation. In *IEEE International Conference on Robotics and Automation (ICRA)*, volume 2, pages 1398–1404, 1991.

[10] Avishai Weiss, Morgan Baldwin, Richard Scott Erwin, and Ilya Kolmanovsky. Model predictive control for spacecraft rendezvous and docking: Strategies for handling constraints and case studies. *IEEE Transactions on Control Systems Technology*, 23(4):1638–1647, 2015.

[11] Qi Li, Jianping Yuan, Bo Zhang, and Chen Gao. Model predictive control for autonomous rendezvous and docking with a tumbling target. *Aerospace Science and Technology*, 69:700–711, 2017.

[12] Courtney Bashnick and Steve Ulrich. Fast model predictive control for spacecraft rendezvous and docking with obstacle avoidance. *Journal of Guidance, Control, and Dynamics*, 46(5):998–1007, 2023.

[13] Pedro Taborda, Hugo Matias, Daniel Silvestre, and Pedro Lourenço. Convex MPC and thrust allocation with deadband for spacecraft rendezvous. *IEEE Control Systems Letters*, 2024.

[14] Andrew Fear and E Glenn Lightsey. Autonomous rendezvous and docking implementation for small satellites using model predictive control. *Journal of Guidance, Control, and Dynamics*, 47(3):539–547, 2024.

[15] Yuanqi Mao, Daniel Dueri, Michael Szmuk, and Behçet Açıkmeşe. Successive convexification of non-convex optimal control problems with state constraints. *IFAC-PapersOnline*, 50(1):4063–4069, 2017.

[16] Tyler M Lovelly, Travis W Wise, Shaun H Holtzman, and Alan D George. Benchmarking analysis of space-grade central processing units and field-programmable gate arrays. *Journal of Aerospace Information Systems*, 15(8):518–529, 2018.

[17] Aaron D Ames, Xiangru Xu, Jessy W Grizzle, and Paulo Tabuada. Control barrier function based quadratic programs for safety critical systems. *IEEE Transactions on Automatic Control*, 62(8):3861–3876, 2016.

[18] Aaron D Ames, Samuel Coogan, Magnus Egerstedt, Gennaro Notomista, Koushil Sreenath, and Paulo Tabuada. Control barrier functions: Theory and applications. In *2019 18th European control conference (ECC)*, pages 3420–3431. IEEE, 2019.

[19] Eduardo D Sontag. A Lyapunov-like characterization of asymptotic controllability. *SIAM journal on control and optimization*, 21(3):462–471, 1983.

[20] Joseph Breeden and Dimitra Panagou. Autonomous spacecraft attitude reorientation using robust sampled-data control barrier functions. *Journal of Guidance, Control, and Dynamics*, 46(10):1874–1891, 2023.

[21] Yu-Yao Wu and Hui-Jie Sun. Attitude tracking control with constraints for rigid spacecraft based on control barrier Lyapunov functions. *IEEE Transactions on Aerospace and Electronic Systems*, 58(3):2053–2062, 2021.

[22] Joseph Breeden and Dimitra Panagou. Guaranteed safe spacecraft docking with control barrier functions. *IEEE Control Systems Letters*, 6:2000–2005, 2021.

[23] Matheus F Reis, A Pedro Aguiar, and Paulo Tabuada. Control barrier function-based quadratic programs introduce undesirable asymptotically stable equilibria. *IEEE Control Systems Letters*, 5(2):731–736, 2020.

Except where otherwise noted, content of this paper is licensed under a Creative Commons Attribution 4.0 International License.

The reproduction and distribution with attribution of the entire paper or of individual pages, in electronic or printed form, including any material under non-CC-BY 4.0 licenses is hereby granted by the authors and respective copyright owners.

[24] Jaskaran Grover, Changliu Liu, and Katia Sycara. Why does symmetry cause deadlocks? *IFAC-PapersOnLine*, 53(2):9746–9753, 2020.

[25] Muhammad Zakiyullah Romdlony and Bayu Jayawardhana. Stabilization with guaranteed safety using control Lyapunov-barrier function. *Automatica*, 66:39–47, 2016.

[26] Philipp Braun and Christopher M Kellett. Comment on "stabilization with guaranteed safety using control Lyapunov–barrier function". *Automatica*, 122:109225, 2020.

[27] Xiao Tan and Dimos V Dimarogonas. On the undesired equilibria induced by control barrier function based quadratic programs. *Automatica*, 159:111359, 2024.

[28] Ricardo G Sanfelice. *Hybrid feedback control*. Princeton University Press, 2021.

[29] Paul Glotfelter, Ian Buckley, and Magnus Egerstedt. Hybrid nonsmooth barrier functions with applications to provably safe and composable collision avoidance for robotic systems. *IEEE Robotics and Automation Letters*, 4(2):1303–1310, 2019.

[30] Alexander Robey, Lars Lindemann, Stephen Tu, and Nikolai Matni. Learning robust hybrid control barrier functions for uncertain systems. *IFAC-PapersOnLine*, 54(5):1–6, 2021.

[31] Philipp Braun, Christopher M Kellett, and Luca Zaccarian. Explicit construction of stabilizing robust avoidance controllers for linear systems with drift. *IEEE Transactions on Automatic Control*, 66(2):595–610, 2020.

[32] Philipp Braun and Luca Zaccarian. Augmented obstacle avoidance controller design for mobile robots. *IFAC-PapersOnLine*, 54(5):157–162, 2021.

[33] Riccardo Ballaben, Philipp Braun, and Luca Zaccarian. Lyapunov-based avoidance controllers with stabilizing feedback. *IEEE Control Systems Letters*, 2024.

[34] Mathias Marley, Roger Skjetne, and Andrew R Teel. Hybrid control barrier functions for continuous-time systems. *IEEE Transactions on Automatic Control*, 2024.

[35] Christopher G Mayhew, Ricardo G Sanfelice, and Andrew R Teel. Synergistic Lyapunov functions and backstepping hybrid feedbacks. In *Proceedings of the 2011 American control conference*, pages 3203–3208. IEEE, 2011.

[36] Christopher G Mayhew, Ricardo G Sanfelice, and Andrew R Teel. Further results on synergistic Lyapunov functions and hybrid feedback design through backstepping. In *2011 50th IEEE Conference on Decision and Control and European Control Conference*, pages 7428–7433. IEEE, 2011.

[37] Hugo Matias and Daniel Silvestre. Hybrid Lyapunov and barrier function-based control with stabilization guarantees. *arXiv preprint arXiv:2504.09760*, 2025.

[38] Lawrence Perko. *Differential equations and dynamical systems*, volume 7. Springer Science & Business Media, 2013.

[39] Eduardo D Sontag. A 'universal'construction of Artstein's theorem on nonlinear stabilization. *Systems & control letters*, 13(2):117–123, 1989.

[40] Benjamin Morris, Matthew J Powell, and Aaron D Ames. Sufficient conditions for the Lipschitz continuity of QP-based multi-objective control of humanoid robots. In *52nd IEEE Conference on Decision and Control*, pages 2920–2926. IEEE, 2013.

[41] Mrdjan Jankovic. Robust control barrier functions for constrained stabilization of nonlinear systems. *Automatica*, 96:359–367, 2018.

Except where otherwise noted, content of this paper is licensed under a Creative Commons Attribution 4.0 International License.

The reproduction and distribution with attribution of the entire paper or of individual pages, in electronic or printed form, including any material under non-CC-BY 4.0 licenses is hereby granted by the authors and respective copyright owners.

[42] Jun Zeng, Bike Zhang, Zhongyu Li, and Koushil Sreenath. Safety-critical control using optimal-decay control barrier function with guaranteed point-wise feasibility. In *2021 American Control Conference (ACC)*, pages 3856–3863. IEEE, 2021.

[43] Tamas G Molnar and Aaron D Ames. Composing control barrier functions for complex safety specifications. *IEEE Control Systems Letters*, 2023.

[44] Pio Ong and Jorge Cortés. Universal formula for smooth safe stabilization. In *2019 IEEE 58th conference on decision and control (CDC)*, pages 2373–2378. IEEE, 2019.

[45] Andrew J Taylor, Pio Ong, Tamas G Molnar, and Aaron D Ames. Safe backstepping with control barrier functions. In *2022 IEEE 61st Conference on Decision and Control (CDC)*, pages 5775–5782. IEEE, 2022.

Except where otherwise noted, content of this paper is licensed under a Creative Commons Attribution 4.0 International License.

The reproduction and distribution with attribution of the entire paper or of individual pages, in electronic or printed form, including any material under non-CC-BY 4.0 licenses is hereby granted by the authors and respective copyright owners.